

Article

The Results and Developments of the Radon Monitoring Network in Seismic Areas

Victorin Emilian Toader^{1,*}, Constantin Ionescu¹, Iren-Adelina Moldovan¹, Alexandru Marmureanu¹, Nicoleta-Sanda Brisan², Iosif Lingvay³ and Andrei Mihai¹

¹ National Institute for Earth Physics, Calugareni 12, 077125 Magurele, Romania; viorel@infp.ro (C.I.); iren@infp.ro (I.-A.M.); marmura@infp.ro (A.M.); mihai.andrei@infp.ro (A.M.)

² Faculty of Environmental Science and Engineering, Babeş-Bolyai University, 400535 Cluj-Napoca, Romania; nicoleta.brisan@ubbcluj.ro

³ S.C. Electrovalcea SRL, Str. Ferdinand 19, 240571 Râmnicu Vâlcea, Romania; iosiflingvay@yahoo.com

* Correspondence: victorin@infp.ro

Abstract: The analysis of the relationship between radon and seismicity was previously carried out in the seismic zone of Vrancea (Romania), positioning the measuring stations on tectonic faults. This article analyzed the evolution of radon under conditions of deep and surface seismicity and the presence of mud volcanoes, as well as fires caused by gasses emanating from the ground. The monitoring area was extended to the Black Sea and the area of the Făgăraş-Câmpulung fault, where a special radon detection system was established and proposed for patenting. The case study was the impact of the earthquakes in Turkey (7.8 R and 7.5 R on 6 February 2023) on the seismically active areas in Romania in terms of gas emissions (radon, CO₂). The main analysis methods for radon (we also included CO₂) were applied to integrated time series and the use of anomaly detection algorithms. Data analysis showed that the effects of global warming led to variations in seasonal gas emissions compared to previous years. This made it difficult to analyze the data and correlate it with seismicity. Several of the cases presented require more in-depth analysis to determine the cause of the unusually high radon levels. The primary purpose of establishing the monitoring network is to use the gas emissions as seismic precursors, but the measurements are affected by the conditions under which the monitoring is conducted. In some cases, we are dealing with the effects of pollution, and in other cases, more extensive studies are required. One solution we plan to use is to expand the measurement points to locate the source of the anomalies and use weather data to determine the impact of global warming on the measurements. The main conclusions related to the development of a radon monitoring network and, in general, to the emission of gasses in earthquake-prone areas relate to the importance of the choice of equipment, monitoring location, and installation method.

Keywords: air ionization monitoring; anomaly detection; multidisciplinary monitoring; OEF (operational earthquake forecasting); precursor phenomena; radon and CO₂ monitoring



Citation: Toader, V.E.; Ionescu, C.; Moldovan, I.-A.; Marmureanu, A.; Brisan, N.-S.; Lingvay, I.; Mihai, A. The Results and Developments of the Radon Monitoring Network in Seismic Areas. *Atmosphere* **2023**, *14*, 1061. <https://doi.org/10.3390/atmos14071061>

Academic Editor: Antoaneta Ene

Received: 22 May 2023

Revised: 13 June 2023

Accepted: 16 June 2023

Published: 22 June 2023



Copyright: © 2023 by the authors. Licensee MDPI, Basel, Switzerland. This article is an open access article distributed under the terms and conditions of the Creative Commons Attribution (CC BY) license (<https://creativecommons.org/licenses/by/4.0/>).

1. Introduction

This article presents the evolution of implementations and results from the development process of a radon monitoring network as part of a multidisciplinary approach by the National Institute of Earth Physics in Romania [1–3]. The main goal is to create an automated seismic forecasting system (OEF—Operational Earthquake Forecasting) based on real-time data such as radon, CO₂, air ionization, telluric currents, magnetic field, ULF-VLF radio waves, and seismic information. Realizations of this type exist each following a certain parameter for detection [4–9], but each solution refers to a certain area that is monitored. The radon level depends on the tectonic stress that induces a deformation of the rocks [10–13], which in turn depends on the environmental factors. For this reason, the use of a trigger threshold per level for anomaly detection is not possible, but a real-time OEF (Operational Earthquake Forecasting) can be implemented

such as in [2]. In [3,5], an application for the Vrancea zone (the curvature area of the Carpathian Mountains) is presented; in [4] is the forecasting is for Japan; Reference [6] used a general monitoring of electromagnetic emissions (EM) (we tried something similar, but the results are not convincing for Vrancea [10]); and Reference [7] prospected for operational forecasting of earthquakes in Europe using seismic information, but the catalogs are not homogeneous and the seismicity patterns are too different for different areas. The authors of the article [8] specify the difference between forecast and prediction, emphasizing the difficulties of using it in general the 'time-dependent seismic hazards to help communities prepare for potentially destructive earthquakes. The main problem of using seismic catalogs is that they reflect more the detection capacity of the respective networks. The most recent example for Romania is Oltenia, Gorj area, where more than 2000 surface earthquakes occurred recently and which was reclassified as a seismic risk area after 200 years (<https://data.mendeley.com/datasets/28kv3gsgcz/2>, accessed on 27 September 2022). The large number of earthquakes is due to the increase in detection capacity as a result of monitoring with a larger number of seismic stations installed in that area. Even if the statistical methods are correct, they are applied on insufficient data, especially when they refer to natural phenomena. Radon monitoring also expanded as a result of the development of monitoring equipment, which depended on technological development in general. Our efforts to integrate real-time radon data were described in [3]. At the current stage, all multidisciplinary information is accessible in real time from a database that has an interface for viewing at gebs.infp.ro (API interface—JSON format, sample data at <https://data.mendeley.com/datasets/28kv3gsgcz/2>, accessed on 27 September 2022). The biggest challenges were the integration of data coming from equipment with different hardware and software interface options, the creation of metadata, the implementation of the database, its management, and access to information. Radon concentration as seismic precursor is mentioned in OEF [9] along the fluctuations of the 'groundwater level, electromagnetic variations near and above the Earth's surface, thermal anomalies, abnormal animal behavior, seismicity models' and with the possibility of generating false alarms.

This paper analyzed the relationship between radon and CO₂ emissions, seismicity, and meteorological conditions, along with several case studies, such as the relationship between recent seismic events in Turkey (7.8 R) and seismicity in Romania, or radon exceedance in some situations. A description of the network (stations, equipment, their positioning, activity periods, measurement results) and metadata can be found in Section 2. A special case is the Râmnicu Vâlcea station, built for radon monitoring (patent application [14]). The analytical methods used are described in [2,3] and are applied to several case studies. The first one refers to the use of radon and CO₂ in the correlation of seismic events in Turkey (7.8 R) and those in the Râmnicu Sărat area (Romania), followed by the analysis of an earthquake sequence from Vrancea with a magnitude of 4.2 R through the prism of gas emissions, a case of pollution at the Black Sea caught during the attempt to monitor the Shabla area, and the exceeding of the value of 300 Bq/mc (the limit set by Council Directive 2013/59/EURATOM) in several situations. We also performed an analysis of the dependence of radon and CO₂ emissions on meteorological factors, seismic energy, and seismicity of Vrancea, represented by parameters a-b of the Gutenberg–Richter law [15,16]. In these cases, we applied correlation and averaging functions to sliding time windows applied to radon time series. The results are comparable to the function-based methods in the LabVIEW programming environment library. One aspect analyzed is the correlation of radon emissions with the characteristics of the Vrancea area, which is characterized by both intermediate earthquakes (unlikely to cause direct gas emissions) and crustal earthquakes. Finally, the analysis of the data from 2016 shows that climate changes cause radon emissions to increase together with temperature.

2. The New Radon and CO₂ Monitoring Network

2.1. The Updated Structure of the Monitoring Network

The first development of a radon detection device for Vrancea was carried out by IFIN HH and installed at the Plostina station (INFOSOC 2006 project—complex system for monitoring and processing precursors of major seismic events by modern techniques, Figure 1). The high radon values in Figure 1 were not confirmed by the measurements performed with a device of the RADON SCOUT type, which was installed in 2017 at the same location and is still working (Table 1).

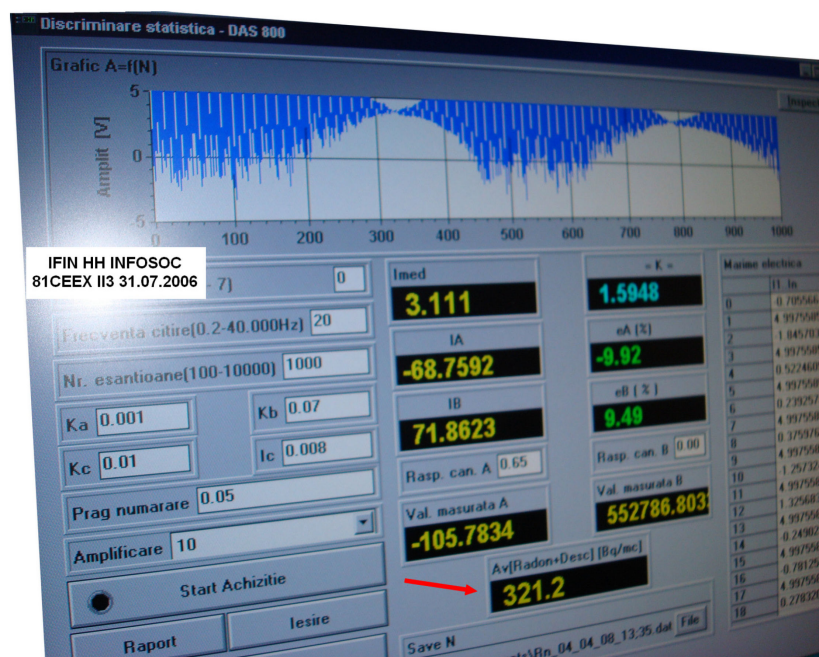


Figure 1. The software for the first development of an experimental radon detection in a seismic zone was created by IFIN HH, 2006.

Concerns about the relationship between radon emission and seismicity have expanded to include a multidisciplinary monitoring network that currently includes gas emission as a precursor parameter [2,3]. Figure 2 (the green markers indicate radon and CO₂, the yellow ones mean radon devices only) and Table 1 show the evolution of the radon monitoring network, to which CO₂ has been added as a seismic precursor [17,18], but also as a parameter for the analysis of greenhouse gas impacts and climate change.

The Carpathian Mountains formed through a process spanning the Triassic to Tertiary periods, involving the transformation of continental units and the closure of Alpine Thetys and its branches. These continental units consist of the Tisza–Dacia and Alps–Carpathian–Pannonian (ALCAPA) blocks, located internally, while externally, there is the European/Scythian/Moesian continental foreland. The arcuate shape of the Carpathians is mirrored by this external foreland [19]. During the Quaternary period, the significant amount of shortening, reaching up to 5 km, was laterally distributed through transcurrent movements along the major faults that delineate the southeastern Carpathians, specifically the Trotus and Intramoesian faults. Notably, there are observable patterns (south to Trotus Fault) of active faulting in close proximity to the boundary between the Moesian platform and the North Dobrogean orogen. These patterns can be attributed to strain partitioning, which occurs due to the differentiation of stress between mechanically weak and strong lithospheric regions, as explained by Matenco et al. in 2007 [20]. As a result of this complex tectonic evolution, the Vrancea zone is characterized by seismic activity from both crustal and intermediate earthquakes, with moderately strong to strong earthquakes occurring more frequently in the intermediate sector. Intermediate seismicity is concentrated in the bend of the Carpathian arc in the Vrancea region. In the intermediate sector, a compressive

regime dominates, leading to reverse faulting and vertical extension [21]. Conversely, crustal earthquakes are influenced by an extensional regime characterized by normal and strike-slip faulting [22]. As it can be seen in Figure 2, we plotted on the map the main faults resulting from the complex tectonic process described above, as well as the distribution of measurement stations. The radon measurement stations are located both near the faults and above the two seismic zones in Vrancea (Intermediate Vrancea and Crustal Vrancea).

Table 1. Radon network, locations, equipment, and period of operation.

Station Names	Location	Equipment	North	East	Description	Start Time	End Time
Agigea	Agigea	RADONSCOUT	44.0838	28.6412	Agigea, radon	31 July 2014	5 September 2014
Chiurus	Chiurus	RADONSCOUT	45.8233	26.1646	Chiurus, radon	18 September 2014	18 September 2014
INFP	Magurele	RADONSCOUT	44.3479	26.0281	INFP radon	12 September 2014	15 September 2014
MLRdd	Muntele Rosu	RADONSCOUT	45.4909	25.9450	MLR, radon	2 November 2015	22 March 2017
ODBdd	Odobesti	RADONSCOUT	45.7633	27.0558	Odbi, radon	24 October 2014	4 August 2015
PLRdd1	Plostina 4	RADONSCOUT	45.8512	26.6498	PLOR1, radon	1 August 2017	28 November 2017
PLRdd2	Plostina 4	RADONSCOUT	45.8512	26.6498	PLOR1, radon	28 November 2017	–
BISRdd	Bisoca	RADONSCOUTp	45.5481	26.7099	Bisc, radon	22 October 2014	20 May 2021
BISRAERd	Bisoca	AERC	45.5481	26.7099	Bisoca, radon	25 February 2021	–
DLMdd	Dalma	RADONSCOUTp	45.3629	26.5965	Dalma, radon	4 July 2022	–
LOPRdd	Lopatari	RADONSCOUTp	45.4738	26.5680	Mocearu, radon	6 August 2015	–
MNGdd	Mangalia	RADONSCOUTp	43.8168	28.5876	Mangalia, radon	20 October 2021	14 April 2022
NEHRdd	Nehoiu	RADONSCOUTp	45.4272	26.2952	NEHR, radon	6 August 2015	–
PANCdd	Panciu	RADONSCOUTp	45.8723	27.1477	PANC, radon	29 September 2021	–
RMGVdd	Râmnicu Vâlcea	RADONSCOUTp	45.1075	24.3770	Electrovalcea, radon	22 August 2020	–
SAHRdd	Sahastru	RADONSCOUTp	45.7266	26.6854	SAHR, radon	20 May 2021	–
SURLdd	Surlari	RADONSCOUTp	44.6777	26.2526	Surlari, radon	10 November 2021	–
VRId	Vrancioaia	RADONSCOUTp	45.8657	26.7277	Vri, radon	23 October 2014	21 July 2020

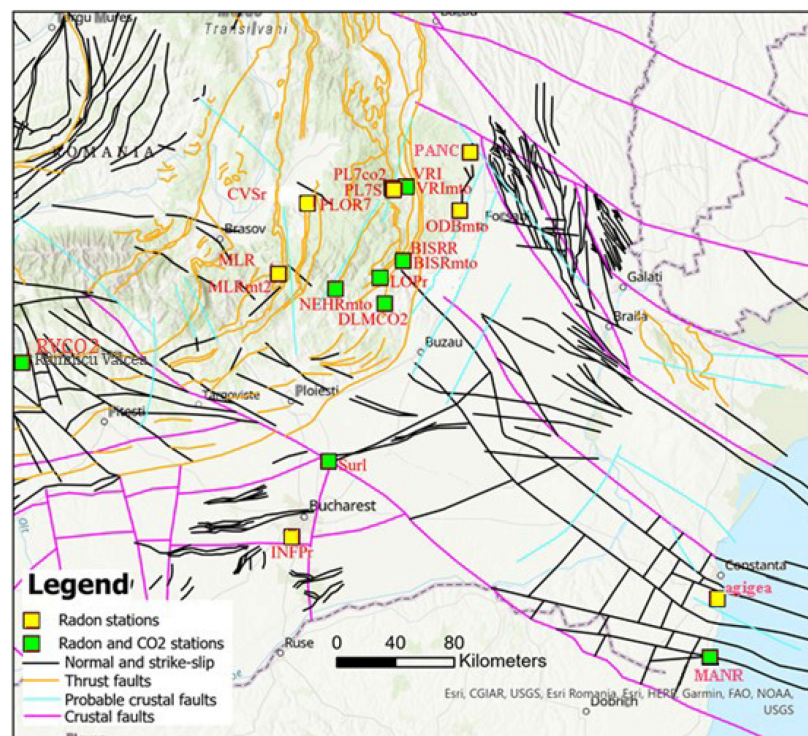


Figure 2. Map of radon and CO₂ monitoring locations; faults are according to Project CEEEX NR.647/2005 CEEEX 647 (C. Dinu, V. Răileanu et al.).

Monitoring stations are located near the faults (Figure 2) because that is where gas emissions are most evident [23–26].

Radon variations are not sufficient to implement a seismic forecasting method. There are other types of devices installed in all monitoring stations. Table 2 shows some of them (CO₂ and weather stations) that contribute to the analysis of seismic precursors besides radon. An example of the analysis of the relationship between radon and CO₂ can be found in the article [27].

Table 2. Equipment that is part of the multidisciplinary monitoring of seismic areas.

Station Names	Location	Equipment	North	East	Per (s)	Description	Start Time	End Time
MLRttu	Muntele Rosu	DL100	45.4909	25.945	1	Tunnel MLR temperature and humidity	5 November 2019	–
LOPrCO2	Lopatari	DL303	45.4738	26.568	1	Lopatari Mocearu CO ₂ /CO	26 June 2019	–
VRico2	Vrancioaia	DL303	45.8657	26.7277	1	Vrancioaia CO ₂ /CO	10 July 2019	21 July 2020
DLMCO2	Dalma	DL303	45.3629	26.5965	1	Dalma CO ₂ /CO	4 July 2022	–
SurlCO2	Surlari	DL303	44.6777	26.2526	1	Surlari CO ₂ /CO	10 November 2021	–
CVSrCO2	Covasna	DL303	45.7944	26.1239	1	Covasna CO ₂ /CO	6 July 2022	–
RVCO2	Râmnicu Vâlcea	DL303	45.1075	24.3770	1	Râmnicu Vâlcea borehole CO ₂ /CO	18 August 2021	13 April 2022
PL7co2	Plostina 7	DL303	45.8603	26.6405	1	PLOR7 CO ₂ /CO	21 July 2020	–
MNGCO2	Mangalia	DL303	43.8168	28.5876	1	Mangalia CO ₂ /CO	20 October 2021	9 March 2022
BISRCO2	Bisoca	DL303	45.5481	26.7099	1	Bisoca CO ₂ /CO	9 July 2019	–
PL7S	Plostina 7	PL7S	45.8603	26.6405	1	PLOR7 solar radiation, K2	14 November 2019	–
BURmto	Bucovina	VANTAGE_PRO2p	47.644	25.2002	60	Bucovina Meteo Vantage	31 October 2018	–
EFORmt2	Eforie Nord	VANTAGE_PRO2p	44.075	28.6323	60	Eforie Meteo Vantage Pro2	2 August 2018	–
INFPmt2	Magurele	VANTAGE_PRO2p	44.3479	26.0281	60	INFP Magurele Meteo DAVIS Vantage Pro2	12 July 2018	–
MetMr2	Marisel	VANTAGE_PRO2p	46.676	23.1189	60	Meteo Davis Marisel	20 July 2018	–
MLRmt2	Muntele Rosu	VANTAGE_PRO2p	45.4909	25.945	60	MLR Meteo DAVIS PRO2+	15 November 2019	–
VRImto	Vrancioaia	WS2355	45.8657	26.7277	60	VRI Meteo, La Crosse 2.0	7 February 2014	–
BISRmto	Bisoca	WS2355	45.5481	26.7099	60	Bisoca, Meteo La Crosse 2.0	25 July 2017	–
NEHRmto	Nehoiu	WS2355	45.4272	26.2952	60	Nehoiu, Meteo La Crosse 20	28 May 2014	–
ODBmto	Odobesti	WS2355	45.7633	27.0558	60	Odobesti, Meteo	21 July 2014	–
PLORmto	Plostina 4	WS2355	45.8512	26.6498	60	PLOR4 Meteo	1 December 2001	–

The description of the data provided by the equipment that measures the radon level (Tables 3 and 4) is included in a general database (<https://data.mendeley.com/datasets/28kv3gsgcz/2>, accessed on 27 September 2022).

Table 3. Radon equipment used in Bisoca station (BISRAERd), produced by ALGADE (discontinued).

Equipment_AERC				
ID	Field 1	Field 2	Field 3	Field 4
1	Radon	Temperature (°C)	Humidity (%)	Status
2	Bq/m ³	°C	%	–
3	%d	%0.1f	%d	%d
4	radon, Radon, temperature in the equipment—Temperature (°C), relative humidity in the equipment—Humidity (%), Sigfox network connection status—Status.			

Table 4. Radon equipment produced by SARAD.

Equipment_RADONSCOUTp							
ID	Field1	Field 2	Field 3	Field 4	Field 5	Field 6	Field 7
1	Radon	Error	Temp	relHum	Pres	Tilt	ROI1
2	Bq/m ³	%	°C	%	mbar	–	cts
3	%d	%d	%0.1f	%d	%d	%d	%d
4	radon, Radon, error—Error, temperature in the equipment—Temp, relative humidity in the equipment—relHum, atmospheric pressure—Press, inclination—Tilt, region of interest 1—ROI1.						

In addition to the location of the monitoring station and the type of equipment used, its installation is also important. The only monitoring station built specifically for this purpose is located in Râmnicu Vâlcea (Electrovalcea SRL site) (Figure 3, RMGVdd in Tables 1 and 5).

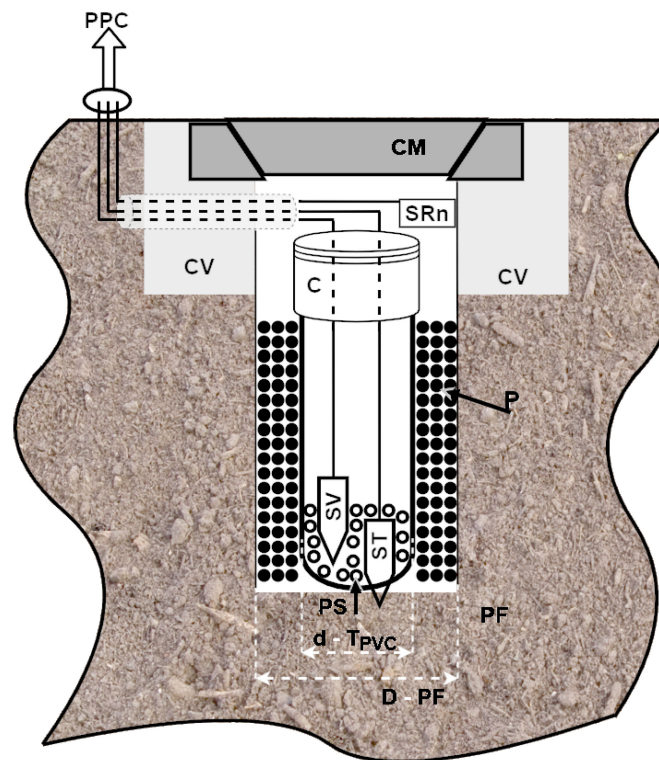


Figure 3. Installation of radon and acceleration sensors in a 40 m deep borehole [14].

The description of Figure 3 according to the patent application “OSIM a 2020 00500 10 August 2020” [14] and the article [28] is as follows:

- PF — Borehole, 40 m deep;
- D — Diameter between 300 and 500 mm;
- SV — Vibration sensor (triaxial accelerometer);
- PS — Glass balls for fixing SV;
- ST — Temperature sensor;
- TPVC — PVC tube;
- C — PVC cover;
- P — 10–30 mm gravel that ensures the diffusion of radon from the bottom of the well to the SRn radon sensor;
- SRn — Radon sensor mounted in the CV visiting space made of reinforced concrete;

- CV — Visiting space;
- CM — Metal cover;
- PPC — Precursor parameters of earthquakes.

More explanations can be found in [28]: ‘According to Figure 3, the vibration transducer SV is mounted between glass beads PS in a drilled well PF 40 m deep and D-PF diameter Φ 350 mm. For the SV protection and of the ST temperature sensor, they are mounted in a PVC protection tube with a diameter of d- TPVC Φ 120 mm. The space between the TPVC and the diameter of the drilled well D-PF is filled with gravel P (1–3 cm), which ensures the diffusion of radon to the radon detector SRn mounted in the manhole CV made of reinforced concrete and covered with a metal cover CM. The PVC T_{PVC} protection tube is covered with a C cover also made of PVC’.

This station was considered a reference because there were no seismic events in the area. Starting with 8 February 2023, over 2000 surface earthquakes occurred at an approximate distance of 80 km in Oltenia, Gorj area (example in Table 7), with the maximum magnitude being 5.7 R. However, no radon level anomalies were recorded in RMGVdd.

Table 5. Synthesized results of radon monitoring, the 2SD reference parameter, and its dependence on temperature.

Station Names	Mean Bq/mc	2SD	Max Bq/mc	Radon—Max Time	Mean T (C)	Max/Min T (C)	Time Interval	
BISRAERd	70.1835	104.1120	500	28 September 2020	17.0133	29.0/−1.5	1 January 2020	31 December 2020
BISRAERd	55.4286	86.2253	498	21 September 2021	15.5043	29.0/+1.5	1 January 2021	31 December 2021
BISRAERd	74.3684	114.6245	432	4 August 2022	16.1838	29.0/−0.5	1 January 2022	31 December 2022
DLMdd	50.1785	82.1935	321	18 October 2022	15.1580	26.5/+1.0	4 July 2022	12 March 2023
LOPRdd	9.5060	14.3086	51	2 October 2020	16.9339	39.5/−3.0	1 January 2020	31 December 2020
LOPRdd	8.6471	12.3745	40	26 June 2021	16.2484	43.5/−1.0	1 January 2021	31 December 2021
LOPRdd	9.1671	15.1524	71	17 May 2022	14.7775	36.5/−1.0	1 January 2022	31 December 2022
PLRdd2	54.0582	66.8106	607	18 June 2020	11.5113	26.5/−1.0	1 January 2020	31 December 2020
PLRdd2	51.3739	84.3485	1068	12 December 2021	10.4853	26.5/−2.5	21/01/01	31 December 2021
PLRdd2	57.0862	135.1785	1077	4 September 2022, 5 September 2022	11.2713	26.5/−1.0	1 January 2022	31 December 2022
MLRdd	518.3502	1090.3606	3230	20 July 2016	7.0435	8.5/+5.5	1 January 2016	31 December 2016
NEHRdd	17.1800	22.7589	75	8 December 2020	16.7921	37.5/−0.5	1 January 2020	31 December 2020
NEHRdd	17.9657	24.0877	71	15 October 2021	15.5227	36.5/−0.5	1 January 2021	31 December 2021
NEHRdd	18.0120	23.9987	71	9 September 2022	16.1370	38.5/−4.5	1 January 2022	31 December 2022
PANCdd	73.5889	216.1618	681	10 December 2022	13.2224	35.5/−7.0	1 January 2022	31 December 2022
RMGVdd	25.1879	26.0728	122	18 June 2021	12.3352	35.0/−6.5	20 October 2021	14 April 2022
RMGVdd	28.0030	25.2148	90	16 August 2022, 17 August 2022	12.8718	35.0/−7.0	1 January 2022	31 December 2022
SAHRdd	87.4349	137.4242	413	29 July 2022, 18 August 2022	20.4269	41.0/+2.5	1 January 2022	31 December 2022
SURLdd	316.9367	320.4041	1095	7 December 2022	13.8398	28.0/−1.5	1 January 2022	31 December 2022
VRIddd	148.8226	157.1080	413	25 January 2018	14.7503	26.0/−3.0	1 January 2018	31 December 2018
VRIddd	165.6702	219.5496	622	5 December 2019	15.7668	29.5/+0.5	1 January 2019	31 December 2019
VRIddd	202.7971	240.1850	642	7 January 2020	15.3096	28.5/+3.0	1 January 2020	21 July 2020
agigea	55.3043	51.5058	115	1 September 2014	21.2522	22.5/21.0	31 August 2014	5 September 2014
MNGdd	313.7032	451.5302	1163	2 December 2021	10.1699	25.0/−3.0	20 October 2021	14 April 2022

2.2. Results of the Radon Monitoring

Table 5 shows the radon monitoring results, including the standard deviation (SD) of the reference parameters and air temperature. The equipment used to determine the radon content also includes sensors for temperature, humidity, and air pressure, i.e., the parameters on which the emission of gasses depends [29,30].

In most cases, the radon anomaly is defined as the positive deviation that exceeds the average radon level by more than two standard deviations, 2SD [31–33]. The temperature

T (C) in Table 5 was measured by the equipment that determines the level of radon. We observed that radon level was over 300 Bq/mc (the limit established by Council Directive 2013/59/EURATOM of 5 December 2013) in MLRdd, SURLdd, and MNGdd. In the first case, the measurements were made in a tunnel in the mountain, which explains the high values. The limit values determined in Surlari (SURLdd) can be explained by the effect of the forest in which the monitoring location is located [34]. In the last case (a case study will follow), Mangalia MNGdd, we recorded very high values and variations of radon, CO₂, and CO. There was a proportional relationship between the radon level and the temperature in the case of the stations BISRAERd, PLRdd2, and RMGVdd (Table 5). In the other stations, this relationship was not preserved, which means that the temperature was not a determining factor in the evolution of the radon level, which depends a lot on the local conditions in which the equipment is installed [34,35]. The fluctuations that occurred were caused by the fact that radon can be brought by the wind from other areas compared to the case of the BISRAERd, PLRdd2, and RMGVdd stations where the spaces where the measurements were made were more isolated.

3. Analysis Methods and Case Studies

The analysis methods used are described in [2,3]. They have been verified with respect to Vrancea seismicity and are currently used for climate change impact analysis. Essentially, the time series representing the gas emissions (radon, CO₂) are integrated after the extraction of the mean, then an algorithm for the detection of STA/LTA (Short-Term Averages/Long-Term Averages) of Allen type ([36–38]) or 2SD (two standard deviations) is applied [33,39]. Signal integration is performed with a function from the LabVIEW library that performs numerical integration using the trapezoidal rule. The Allen detection algorithm is used in earthquake early warning systems but could also be applied to other time series. The standard deviation is a common method for determining radon anomalies. The average radon concentration is the reference value. If radon exceeds the values of ± 2 SD, an event is present. These methods are limited because they depend on the time intervals chosen (daily, seasonal, and annual).

3.1. Case Study: Sequence of Surface Earthquakes, Râmnicu Sărat Area

An example of a case in which these methods are applied is the sequence of surface earthquakes in the area of Râmnicu Sărat (city in Romania), which could have been induced by the seismic events in Turkey (6 February 2023, 7.8 R and 7.5 R, Figure 4) that overlapped (Table 6). This is possible if the earthquakes are above 7 R: ‘Earthquakes, particularly large ones, can trigger other earthquakes in more distant locations through a process known as dynamic stress transfer/triggering’ but should be checked in our case. (<https://www.usgs.gov/faqs/can-large-earthquake-trigger-earthquakes-distant-locations-or-other-faults>, accessed on 10 June 2023).

Table 6 shows that the first seismic event in Turkey (6 February 2023, 01:17:36, 7.8 R) was shortly followed by an earthquake in Romania (6 February 2023, 01:26:20, 4.6 R) at a distance of 1228 km.

Figure 5 (top right) shows the distribution of earthquakes in the period 1 January 2023–12 March 2023, and the A–N section is described in F. Hauser et al., ‘VRANCEA99-. The crustal structure beneath the Southeastern Carpathians and the Moesian platform from a seismic refraction profile in Romania’ (Figure 6).

The closest radon and CO₂ monitoring stations are in Dalma (DLMdd), Bisoca (BISRAERd), and Lopatari (LOPRdd) (Table 1). Applying the mentioned methods, we obtained the evolution of radon and CO₂ as in Figure 7. Only for LOPRdd did we use the 2SD detection method [33], while for the others, we used STA/LTA. It was observed that radon and CO₂ had similar variations, and those in Bisoca and Dalma were similar, unlike those in Lopatari. Moreover, the detections (marked with red dots) can be associated with groups of earthquakes, and the seismic pause that preceded the sequence of earthquakes was longer (seismic quiescence of 7 days [17]). In conclusion, the first seismic event in Turkey could

only have triggered what is happening anyway, with the Râmnicu Sărat area being known for such behavior.

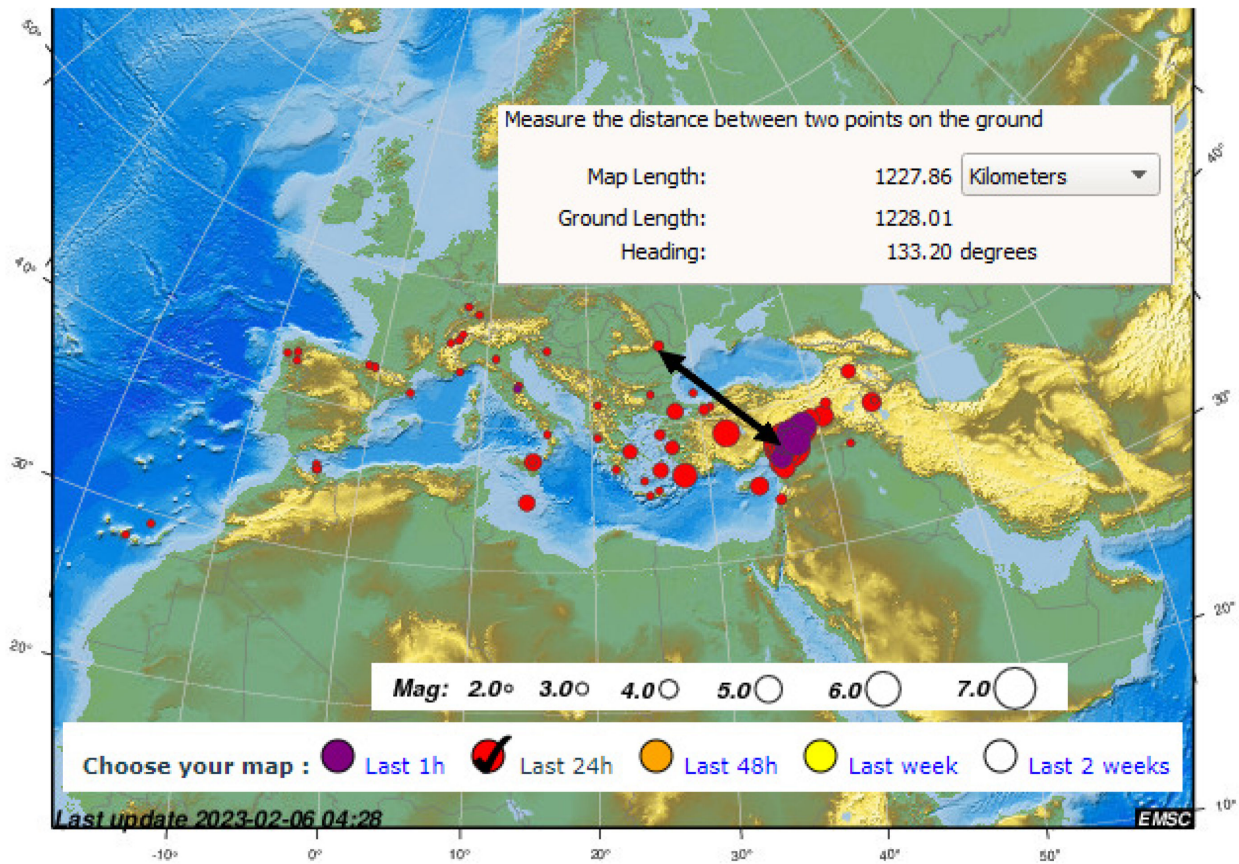


Figure 4. Superposition of the earthquake swarm in Romania with the seismic events in Turkey (6 February 2023, 7.8 R and 7.5 R), picture EMSC/CSEM, <http://www.emsc-csem.org/>, accessed on 6 February 2023.

Table 6. Overlap of earthquakes in Turkey and Romania (<http://www.infp.ro/>, accessed on 21 May 2023).

Data (UTC)	Mag.	Reg.	h (km)
6 February 2023, 10:51:41	5.6 mL	CENTRAL TURKEY	10 km
6 February 2023, 10:24:53	7.5 mL	CENTRAL TURKEY	10 km
6 February 2023, 06:55:14	5.0 mL	CENTRAL TURKEY	10 km
6 February 2023, 03:26:19	2.0 mL	VRANCEA SEISMIC ZONE, BUZAU	21 km
6 February 2023, 03:01:58	2.7 mL	VRANCEA SEISMIC ZONE, BUZAU	17 km
6 February 2023, 02:40:31	2.1 mL	VRANCEA SEISMIC ZONE, BUZAU	13 km
6 February 2023, 02:13:10	2.9 mL	VRANCEA SEISMIC ZONE, BUZAU	17 km
6 February 2023, 02:09:54	2.6 mL	VRANCEA SEISMIC ZONE, BUZAU	17 km
6 February 2023, 01:26:20	4.6 mL	VRANCEA SEISMIC ZONE, BUZAU	22 km
6 February 2023, 01:17:36	7.8 mL	CENTRAL TURKEY	10 km

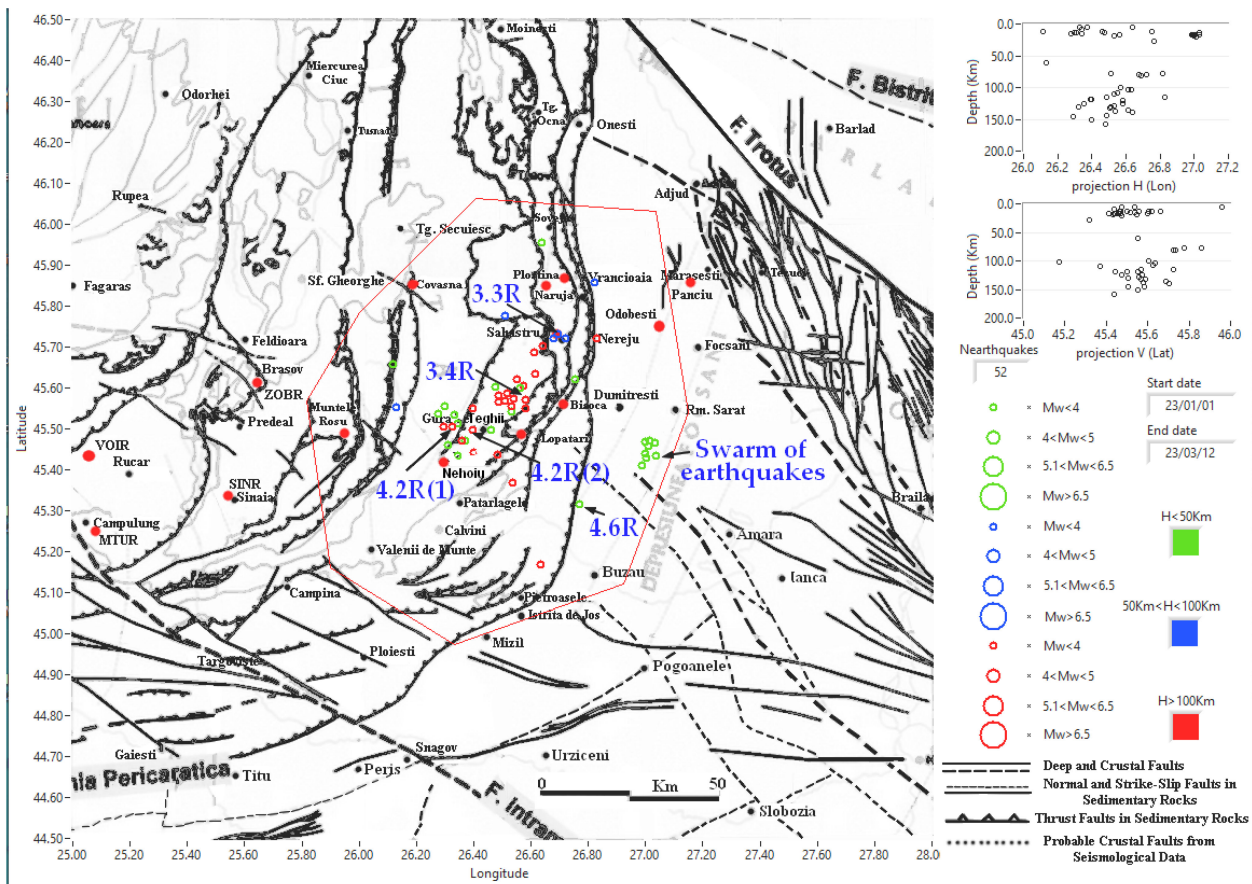


Figure 5. Vrancea seismicity and the correlation of epicenters with geological faults, 1 January 2023–12 March 2023; swarm of Râmnicu Sărat earthquakes (green circles) and 4.2 R earthquakes sequence; faults are according Project CEEEX NR.647/2005 CEEEX 647 (C. Dinu, V. Răileanu et al.).

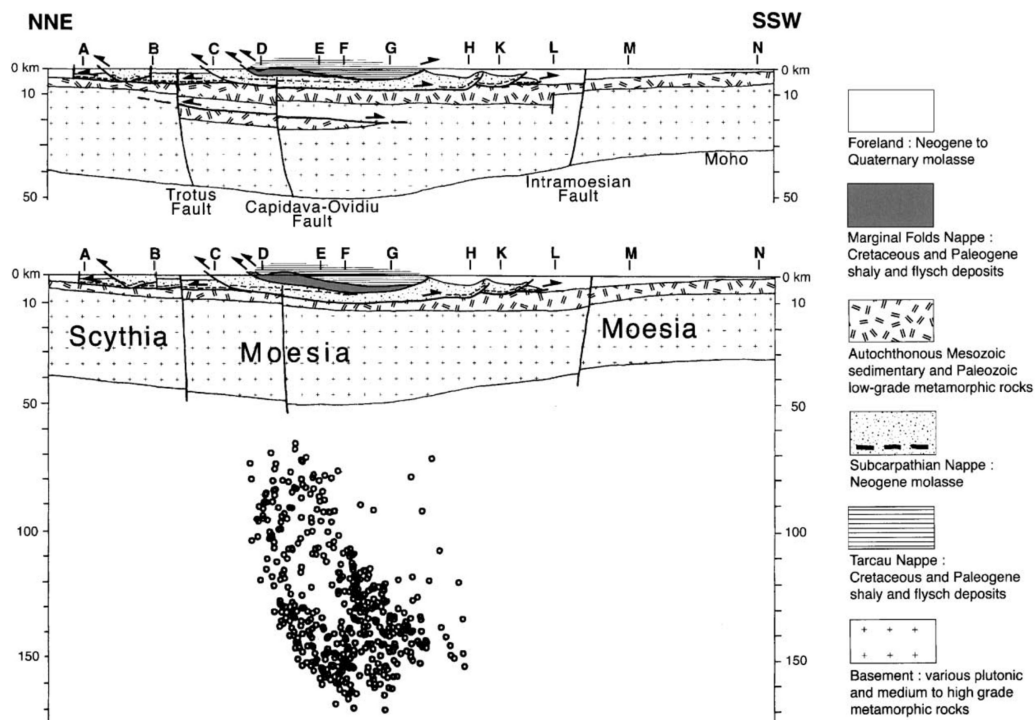


Figure 6. Pre-1999 geological section along the main NNE–SSW VRANCEA99 [40].

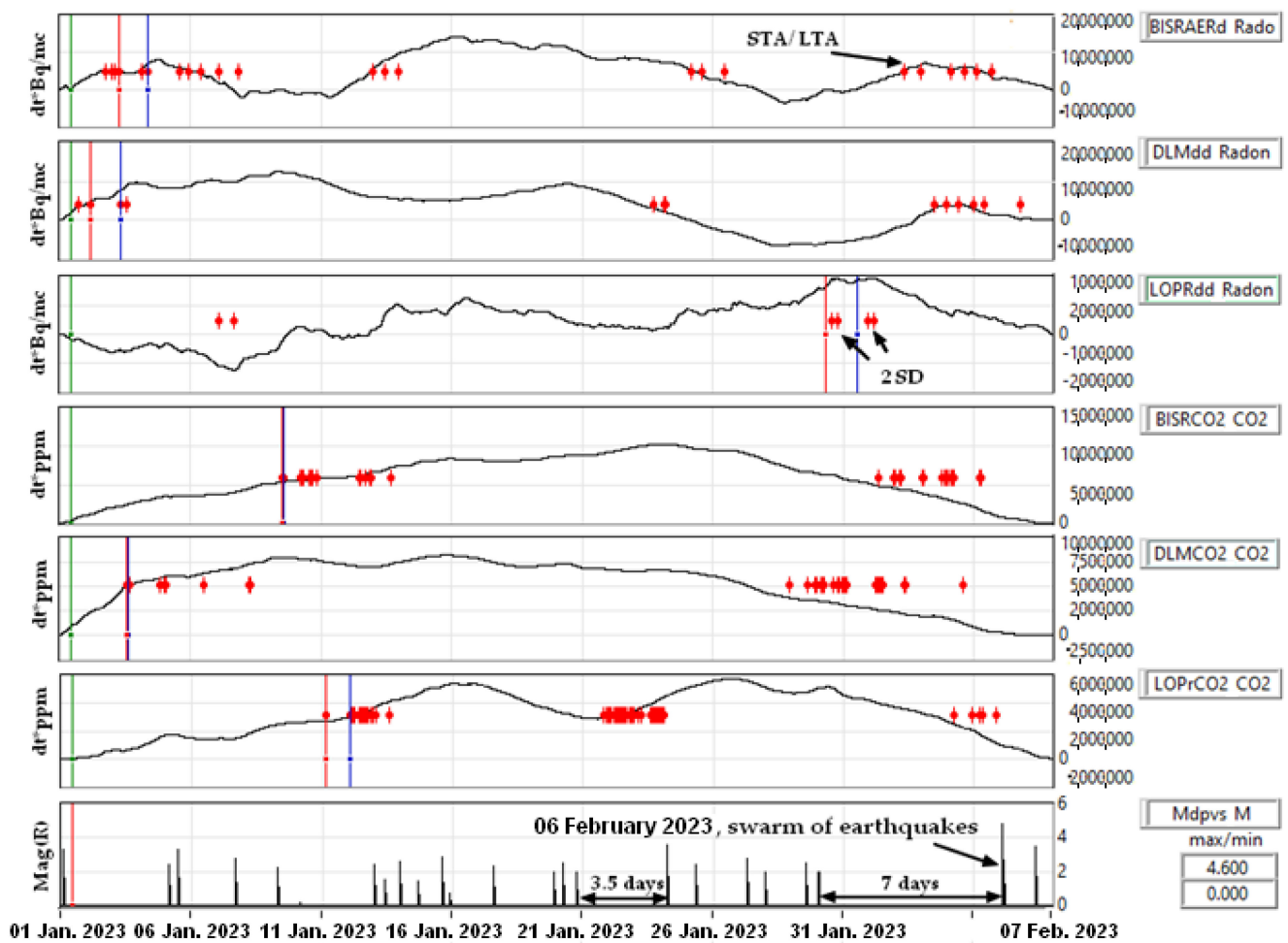


Figure 7. The evolution of radon and CO₂ preceding the earthquake sequence near Râmnicu Sărat, detections marked with red dots.

3.2. Case Study: Earthquakes Sequence 4.2 R

Another case study is the earthquakes sequence from 11 March 202 to 12 March 2023 in which we had two earthquakes of 4.2 R accompanied by two others of 3.3 R and 3.4 R. These are presented in Figures 5 and 8, and Table 7.

The 4.2 R earthquakes were located in the Gura Teghii seismic zone, and all epicenters were on faults (Figure 5). The detections starting with 20 February 2023 in Figure 8 (red points) were of the STA/LTA type and were applied to the integrated time series. There was a similarity in time variations between radon in BISRAERd, DLMdd, and carbon dioxide in DLMCO2 (maximum during 20 February 2023 followed by a decrease). Moreover, the evolution of radon in LOPRdd was similar to CO₂ in BISRCO2 and LOPrCO2.

We can say that the method described in [1,2] is also verified in this case, and what matters is the grouping of earthquakes in a short period of time (1–2 days), even if their magnitude is not high.

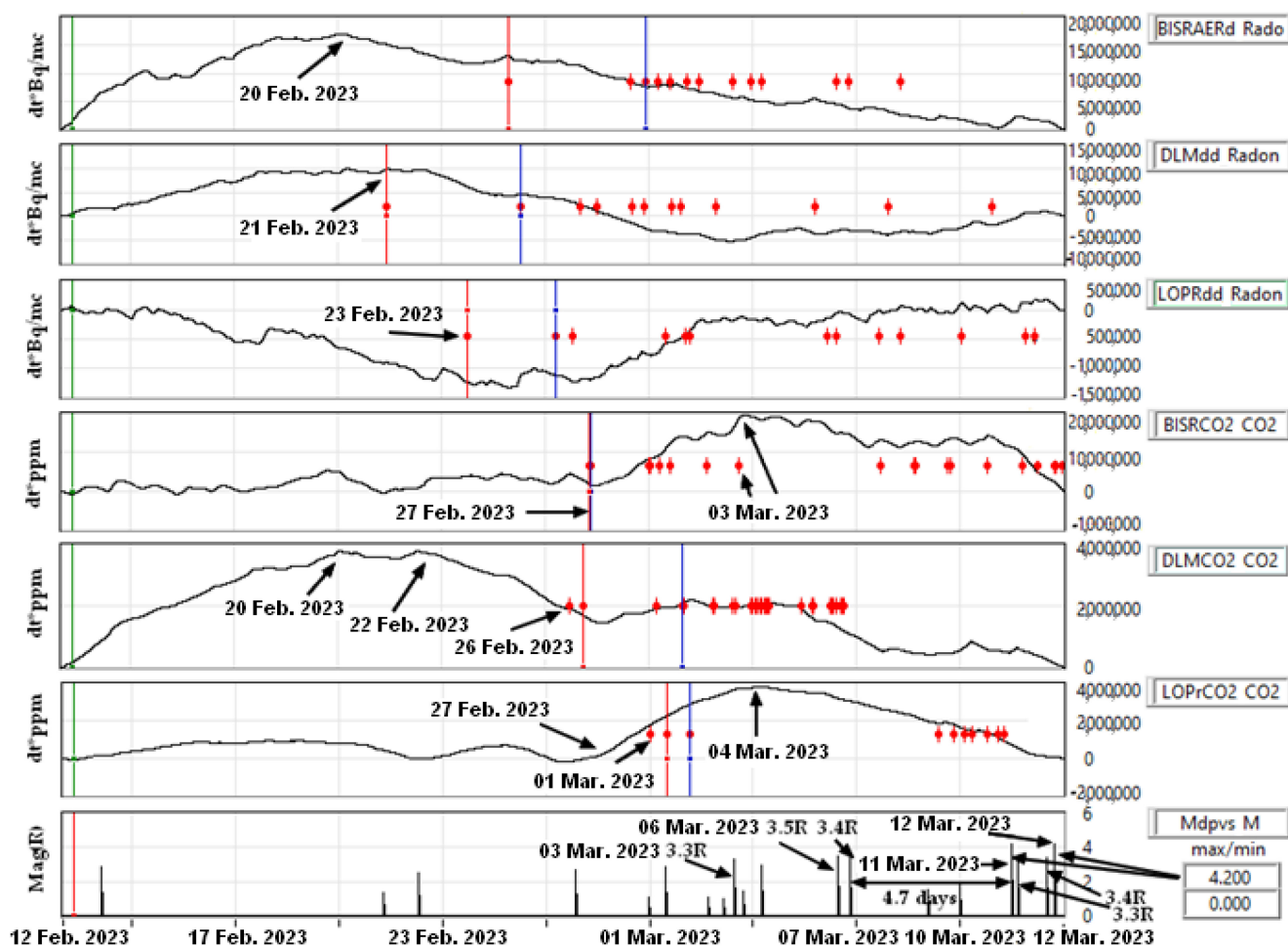


Figure 8. The evolution of radon and CO₂ for the 4.2 R earthquakes sequence, detections marked with red dots.

Table 7. Seismic sequence in the Vrancea area, maximum M 4.2 R, swarm of earthquakes in Oltenia, Gorj.

Data (UTC)	Mag.	Reg.	h (km)
12 March 2023, 19:12:12	2.5 mL	OLTENIA, GORJ	13 km
12 March 2023, 17:44:22	4.2 mL	SEISMIC AREA VRANCEA, BUZAU	131 km
12 March 2023, 12:15:09	3.6 mL	OLTENIA, GORJL	16 km
12 March 2023, 11:49:23	3.4 mL	SEISMIC AREA VRANCEA, BUZAU	125 km
11 March 2023, 20:12:55	2.2 mL	OLTENIA, GORJ	15 km
11 March 2023, 17:51:56	2.6 mL	OLTENIA, GORJ	14 km
11 March 2023, 15:53:22	3.3 mL	SEISMIC AREA VRANCEA, BUZAU	82 km
11 March 2023, 14:17:06	3.5 mL	OLTENIA, GORJ	17 km
11 March 2023, 13:28:57	2.5 mL	OLTENIA, GORJ	16 km
11 March 2023, 13:25:46	2.4 mL	OLTENIA, GORJ	15 km
11 March 2023, 12:09:20	4.2 mL	SEISMIC AREA VRANCEA, BUZAU	118 km

3.3. Case Study: Pollution and Gas Emissions

The next analyzed case refers more to environmental pollution than to a relationship between gas emission and seismicity. In Table 5, the last two stations (named Agigea, Agigea locality, and MNGdd, Mangalia locality) refer to the results of radon monitoring

at the Black Sea (their positioning is in Table 1). A large difference was observed in the level of radon caused by MNGdd, while in Agigea, the radon values were normal (Table 5). However, the time periods in which the determinations were made should be noted. Those in Mangalia were recent and may have been affected by the development of the city and the port. Not only the high values attracted our attention, but also the way in which the gas emission varied in this location. In Figure 9, there are very large variations of radon that did not repeat at intervals of one day and did not depend on temperature, atmospheric pressure, precipitation, or wind (EFORmt2 is a meteorological station, Table 2). Besides these, the presence of CO and the way it varied indicated a pollution that can be caused by the activity of the port, a hospital, or the nearby water treatment plant. The radon measurements at the Black Sea were described in [41], wherein the emission of gases (radon, CO₂, methane, hydrogen sulfide) was specified and analyzed, but not in the coastal region of Romania.

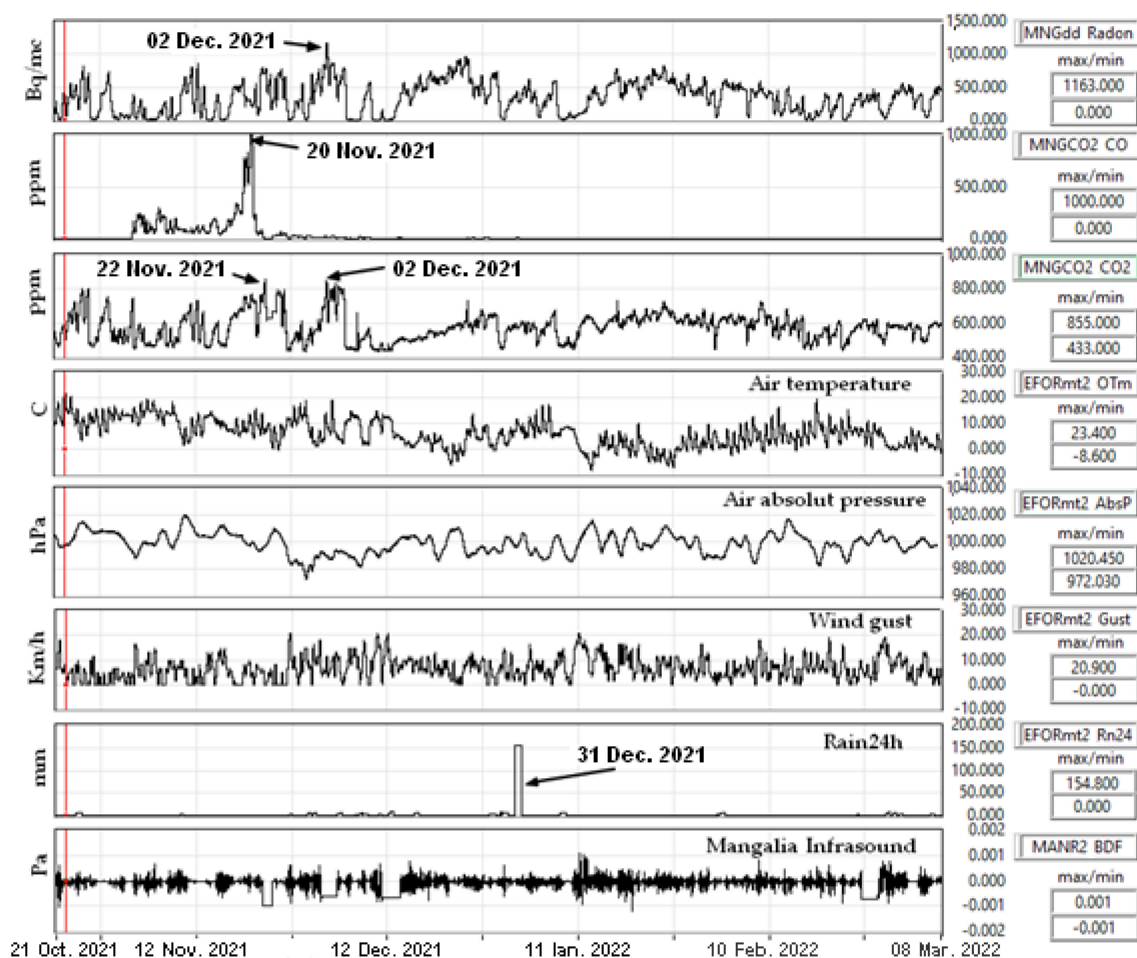


Figure 9. The case of Mangalia: the evolution of radon, CO₂, and atmospheric conditions.

3.4. Case Study: Radon Exceed Limit 300 Bq/mc

Another case to which our attention is drawn in Table 5 is the fact that the radon level in the Surlari station (Figure 10, SURLdd) exceeded the limit of 300 Bq/mc established in Council Directive 2013/59/EURATOM. The building where the radon detector was located is made of bricks and is located in a forest (Figure 10b).

The evolution of radon and CO₂, maximum and minimum values, along with temperature and humidity in this location are presented in Figure 11.

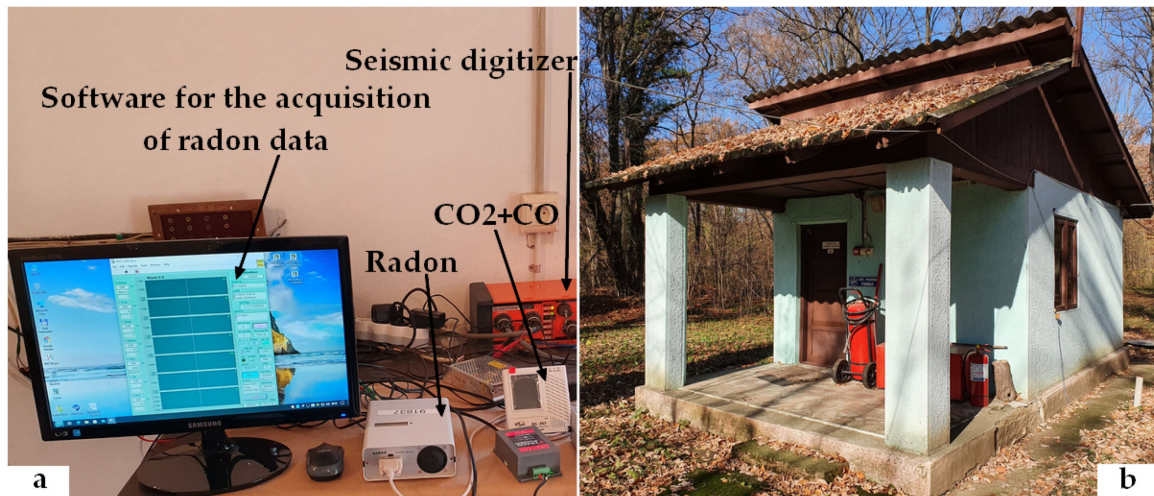


Figure 10. Surlari monitoring station: (a) radon, CO₂, and CO equipment; (b) the location is in a forest.

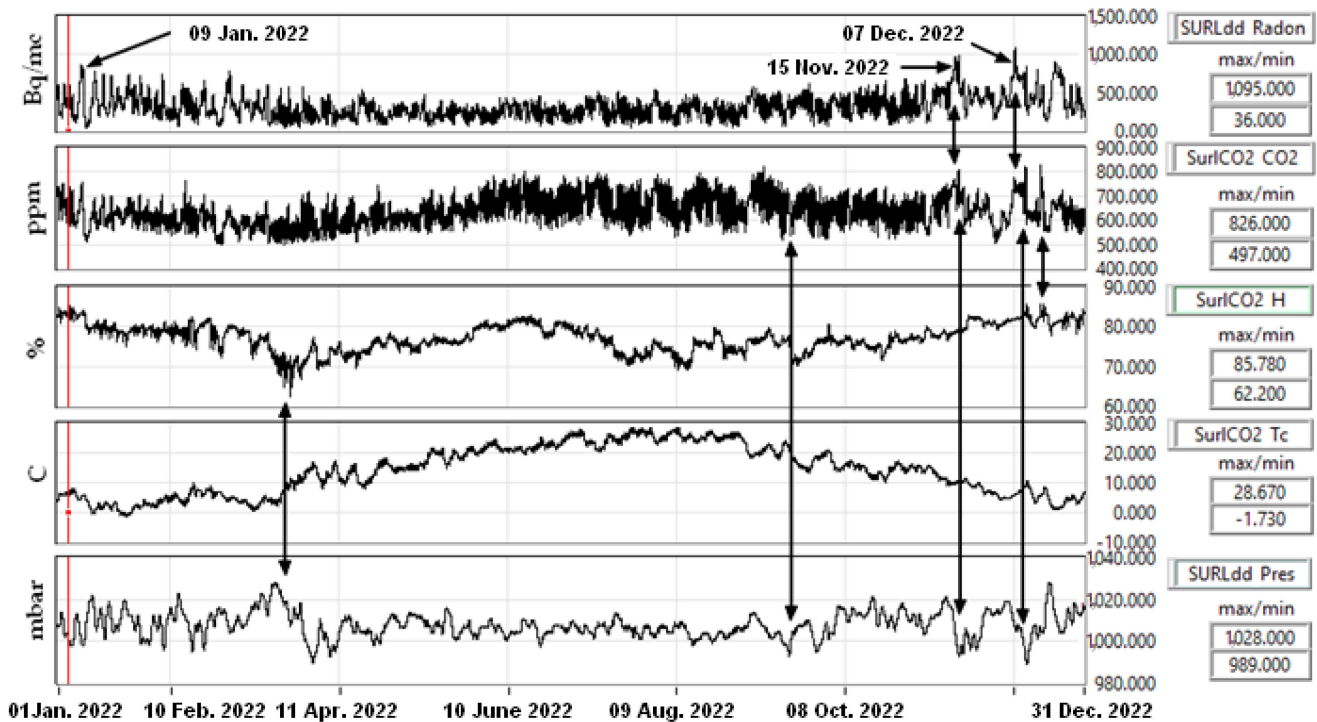


Figure 11. Radon, CO₂, temperature, and air pressure in Surlari station (SURLdd).

It was observed that there was a relationship between the radon level and temperatures in the sense that during the winter, the radon emission increased. The Surlari location is close to the Intramoesica fault and is characterized by surface seismicity. It was observed that there was a relationship between the radon level, temperature, humidity, and atmospheric pressure [42–44]. Seasonal variation indicated an increase in radon emission in winter (lower temperatures), while CO₂ increased in summer (higher temperatures). The daily variations of radon indicated a maximum around 10 UTC hour and a minimum approximately at 19 UTC hour. After filtering with a median filter (LabVIEW library) on the time series from Figure 11 for reducing the daily variations and spikes, we applied a cross-correlation function (LabVIEW library) and obtained the average values from Table 8 (example in Figures 12 and 13). Regardless of the chosen method, it is important that it is used under the same conditions in all the analyzed cases. So, Table 8 is relative to this method over the entire time period (one year) and allows for comparative data analysis.

The possible high values of radon and CO₂ levels were the relation between gas emission and vegetation [34]. The operation of the equipment was checked under normal conditions, and the results were satisfactory. The sensors in Figure 10 were moved because the room where the measurements were taken was not the best location for determining the source of radon or CO₂.

Table 8. Cross-correlation coefficients.

Radon/2022	Station Code						
Mean Cross-Correlation	SURLdd	LOPRdd	NEHRdd	PANCdd	RMGVdd	SAHRdd	BISRAERd
CO ₂	0.3354	0.2758	-0.1701	-	-	-	0.1789
Humidity	0.4430	0.3696	0.2531	0.5708	0.1814	-0.2932	0.2504
Temperature	-0.4181	0.3900	0.1370	-0.2294	0.1467	0.7436	0.4714
Atmospheric pressure	0.0797	0.2313	-0.0152	0.0088	-0.0343	-0.1636	-0.0946

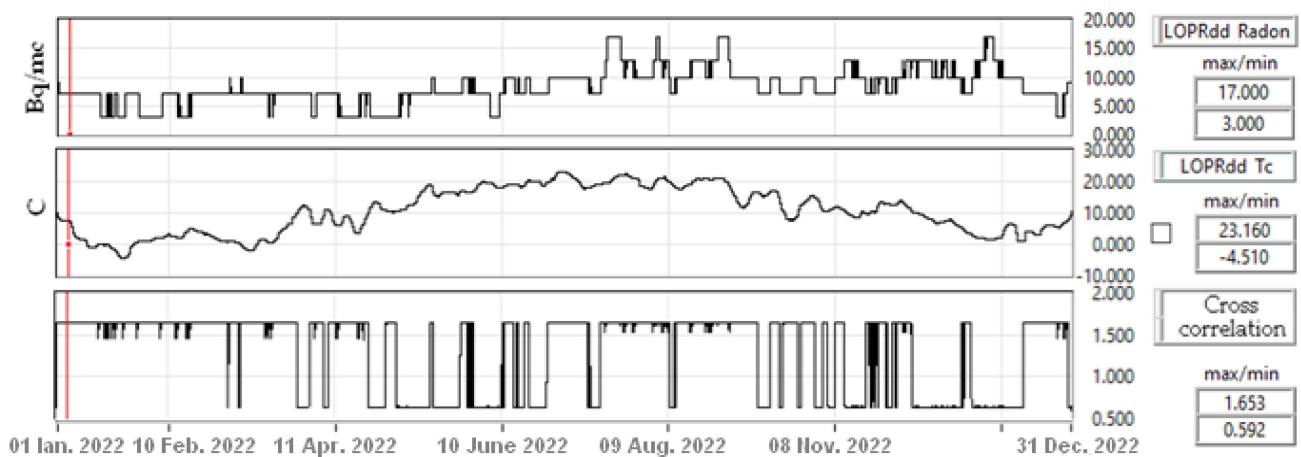


Figure 12. Cross-correlation between radon and humidity in Lopatari station, 2022, 1 h intervals.

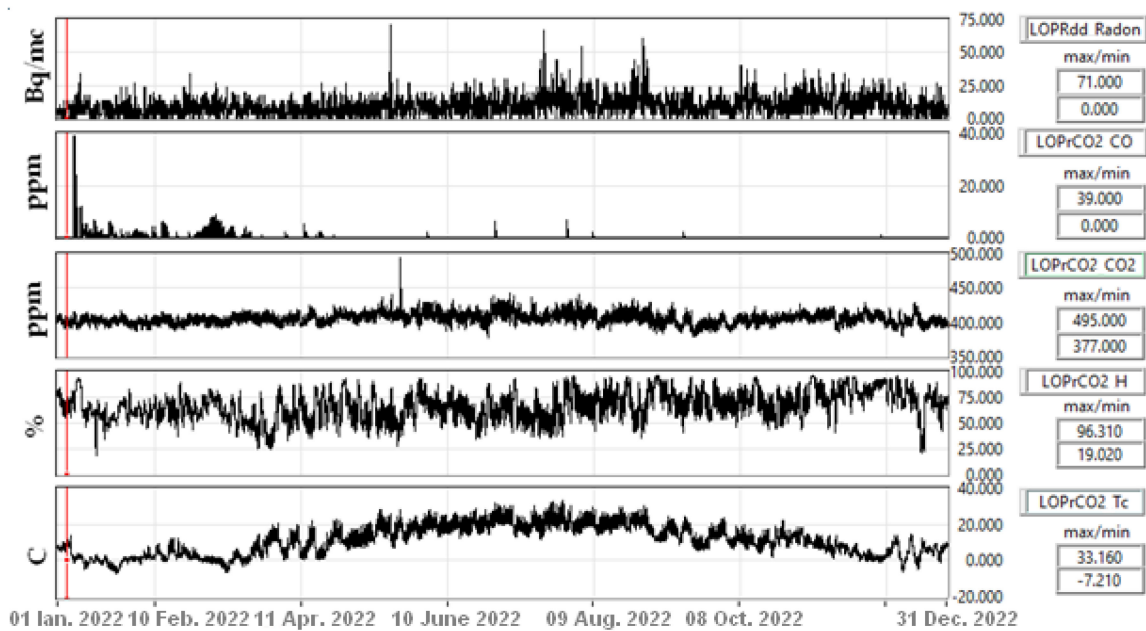


Figure 13. Gas emissions in Lopatari, 2022.

3.5. Case Study: Influence of Meteorological Parameters on Gas Emissions

Another issue is the influence of meteorological parameters on gas emissions, which is presented in many articles [42,45,46]. For our case study, we chose the same time period (year 2022) as in Figure 11 to follow the evolution of radon and CO₂ as a function of temperature, humidity, and atmospheric pressure. Table 8 shows the correlation between radon and CO₂, humidity, temperature, and atmospheric pressure (the complementary parameters measured by the same instruments) for the year 2022.

We notice in Figure 11 that there were correlations over short time intervals. We redid the comparative analysis for the year 2022 but at on a sliding time window of one hour and calculated the average of the obtained coefficients (Table 9). If a positive correlation prevailed, then we would have higher positive final values. However, we could also have an inverse correlation (the sizes are inversely proportional) that would lead to mostly negative results. The way in which the method is applied is represented in Figure 12. So, the values in Tables 9 and 10 are relative and allow for an assessment of the dependence of radon on atmospheric factors.

Table 9. Cross-correlation for time windows of 1 h.

Radon/2022 1 h	Station Code						
	Mean Cross-Correlation	SURLdd	LOPRdd	NEHRdd	PANCdd	RMGVdd	SAHRdd
CO ₂	0.5257	0.6222	0.3742	-	-	-	0.5791
Humidity	0.6385	0.6959	0.6321	0.7216	0.5371	0.3966	0.6902
Temperature	0.3048	0.6529	0.5702	0.3742	0.5663	0.7545	0.6999
Atmospheric pressure	0.5753	0.5892	0.4674	0.5691	0.4569	0.3818	0.4807

Table 10. Vrancea seismicity for earthquakes greater than 4.5 R, 2016–2022.

N	Time	MI > 4.5	Depth	Longitude	Latitude	Mw	P Zone
		Richter	km	Degrees	Degrees		
1	23 September 2016 23:11:20	5.8	92.0	26.6181	45.7148	5.52	236.8
2	27 December 2016 23:20:56	5.8	96.9	26.5987	45.7139	5.52	236.8
3	8 February 2017 15:08:21	5.0	124	26.2886	45.4791	4.6	95.3
4	19 May 2017 20:02:45	4.7	120.6	26.7581	45.7249	4.32	72.3
5	1 August 2017 10:27:52	4.6	96.6	26.4681	45.5146	4.24	66.3
6	2 August 2017 02:32:13	4.9	132.5	26.4014	45.5267	4.51	86.7
7	14 March 2018 10:24:49	4.6	139.1	26.5850	45.6759	4.24	66.3
8	25 April 2018 17:15:49	4.6	147.3	26.4216	45.6002	4.24	66.3
9	28 October 2018 00:38:11	5.8	151.3	26.3986	45.6049	5.52	236.8
10	3 September 2019 11:52:53	4.5	116.7	26.2896	45.4712	4.15	61.0
11	31 January 2020 01:26:48	5.2	120.6	26.7033	45.7106	4.80	116.4
12	24 April 2020 22:04:19	5.0	21.6	27.4651	45.8951	3.79	42.8
13	2 June 2020 11:12:58	4.5	101.2	26.5548	45.6239	4.15	61.0
14	9 April 2021 18:36:47	4.5	77.1	26.6292	45.7916	4.15	61.0
15	25 May 2021 21:30:37	4.7	130.9	26.5226	45.5321	4.32	72.3
16	1 September 2021 10:32:12	4.5	145.0	26.4474	45.6413	4.15	61.0
17	3 November 2022 04:50:26	5.3	148.8	26.5166	45.4949	4.91	129.4
18	17 December 2022 05:42:59	4.5	140.0	26.4668	45.6359	4.15	61.0

3.6. Case Study: CO Can Be a Seismic Precursor

A special case in Lopatari is CO as a result of fire gasses produced by live fires (Figure 13). The time series used in Tables 8 and 9 are shown in Figures 13 and 14. In general, temperature and humidity were inversely proportional (an example in Figure 13 for the Panciu station, PANCdd). This, as well as the dependence of radon on atmospheric factors, depends on the type of installation of the equipment. It can be seen from Table 8 that the dependence of radon on temperature in Lopatari (LOPRdd) was very low, since the measurements were performed with the same equipment (Radon Scout Plus), which was located in a partially air-conditioned room space. For this reason, the relationship between temperature and humidity deviated from normal conditions (Figure 13) (for example, in Panciu, Figure 14). A similar situation existed in Bisoca (BISRAERd).

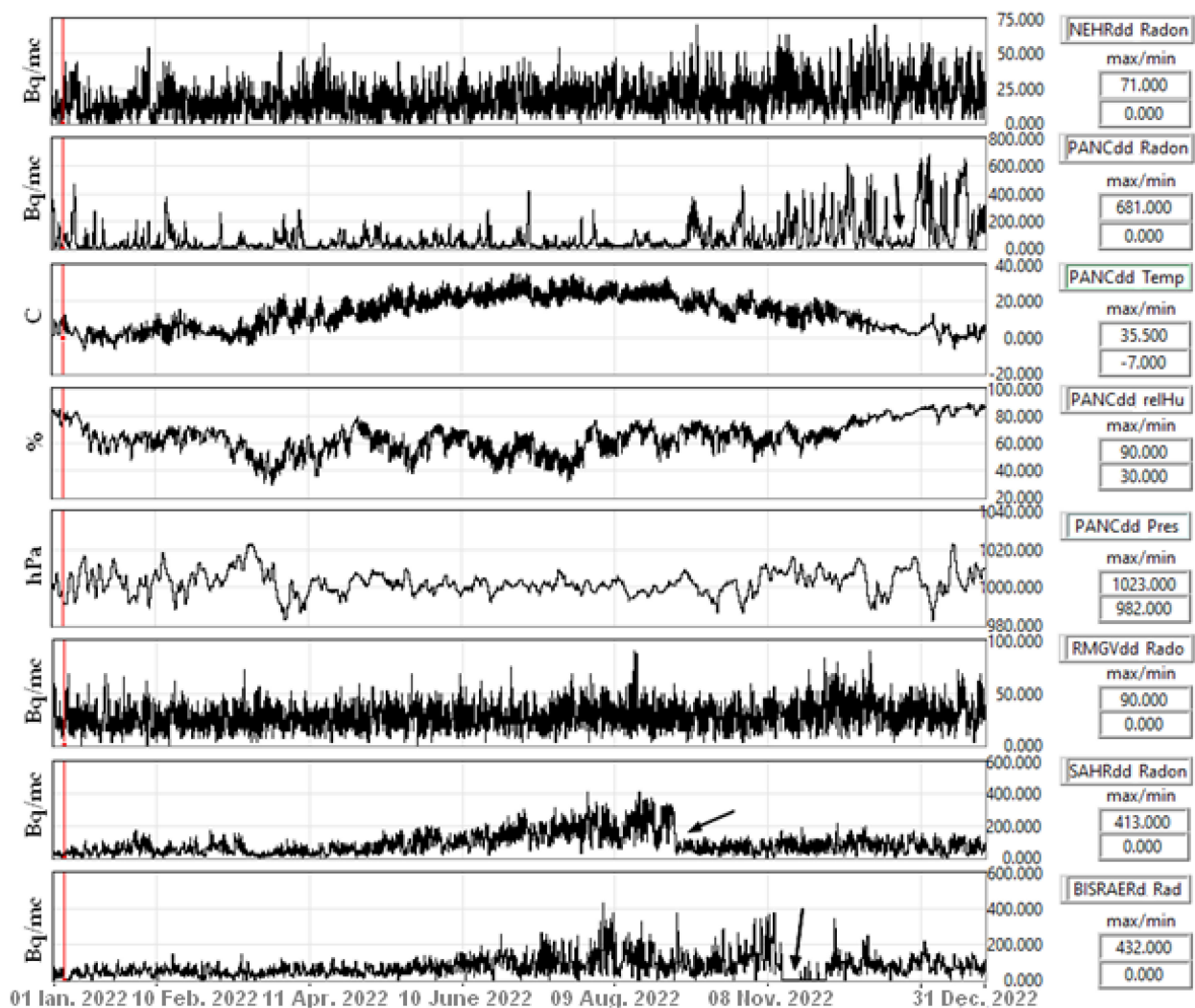


Figure 14. Dependence of radon on atmospheric factors, 2022.

Laboratory measurements of radon highlighted the same direct positive relationship between radon emission and temperature [10]. This is valid if the radon emission and its measurement are done in the same place. In our locations, the rooms where the equipment are placed are not hermetically sealed, and radon can come from nearby areas as a result of air currents. From Figures 11, 13 and 14, a similar evolution of radon can be observed in LOPRdd, RMGVdd, SAHRdd, and BISRAERd (higher values in summer) and for SURLdd, NEHRdd, and PANCdd (higher values in winter). These results are preserved if we analyze the evolution of radon over several years (Figure 15).

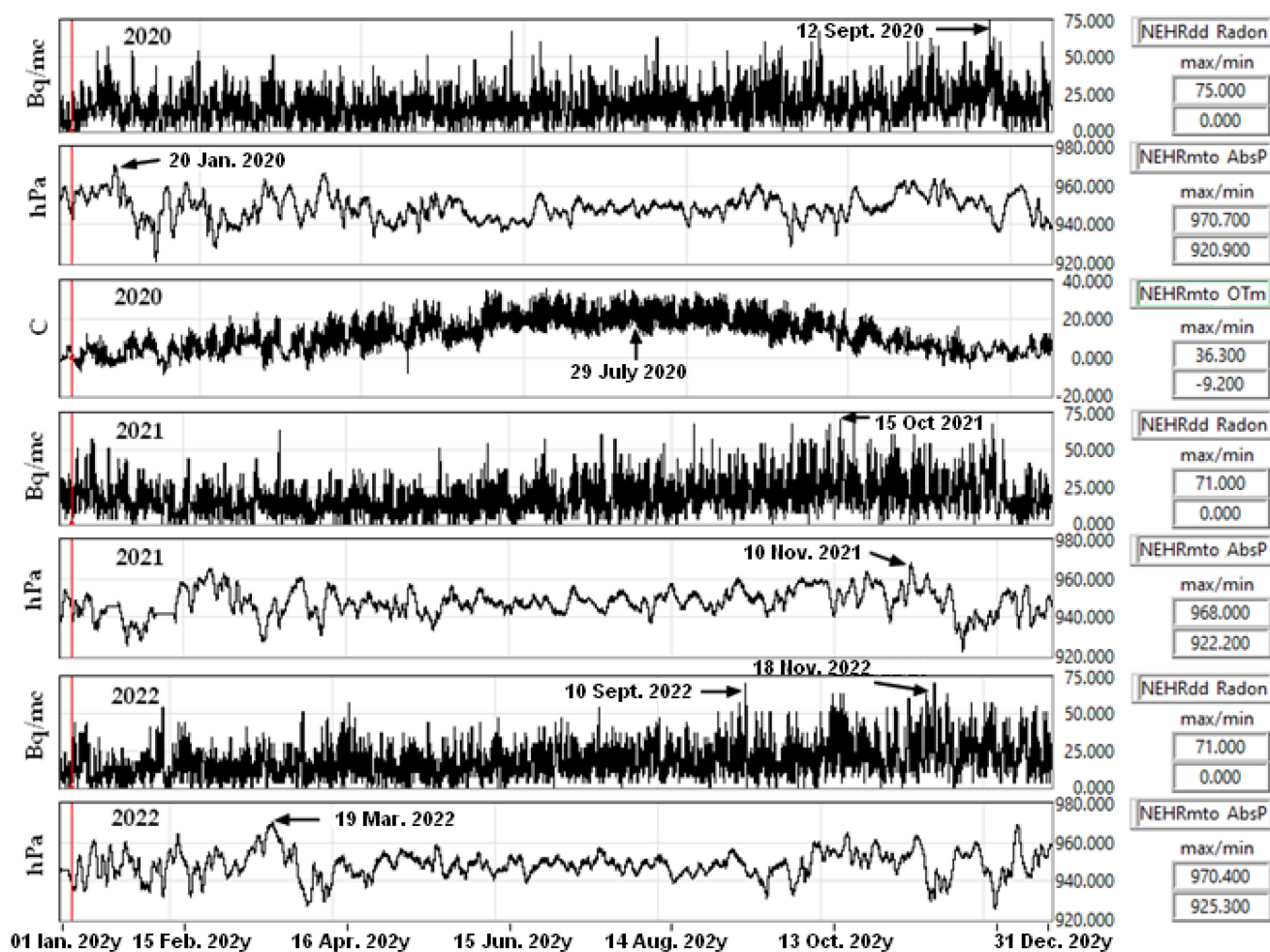


Figure 15. The annual evolution of radon in Nehoiu (NEHRdd) and environmental factors.

3.7. Case Study: Radon Emission and Seismicity

The next case analyzed concerns the relationship between radon emission and seismicity. We already analyzed the Râmnicu Sărat case (Table 6, Figure 7) and the 11 March 2023–12 March 2023 earthquake series (Table 7, Figure 8). We next chose a longer period between 2016 and 2022 and earthquakes larger than 4.5 R in the Vrancea area (Table 10). The preparation zone PZone was determined by the relationship of Dobrovolsky [47] as a function of magnitude. The relation was experimentally verified with M_w . The monitoring station should be located in this area to assess a relationship between radon and earthquakes. Different formulas for the relationship between earthquake magnitude and preparation distance by different authors were mentioned by Nevinsky in [41]. In general, this condition is satisfied in Table 10, since we chose a threshold value of 4.5 R for the magnitude. The relationship between the accumulated seismic energy, the parameters a-b from the Gutenberg–Richter law [15,16], the seismicity, and the number of earthquakes generated in a 7-day interval is shown in Figure 16.

From Figures 16 and 17, it can be seen that a decrease over a period of more than 18 days of the parameter ‘b’ from the Gutenberg–Richter law (GR_b) was followed by earthquakes with a magnitude greater than 5 R (observation valid for the Vrancea area). The radon and temperature time series in Figure 17 were averaged to mitigate daily variations. We note that the maximum values of radon levels were between August and November and did not correlate with the number of earthquakes produced at 7-day intervals (Neq/dt graph). We applied a correlation function between parameter ‘b’ from the Gutenberg–Richter law (GR_b) and radon for the period 2016–2022 for the case where the depth of the hypocenter was greater than 20 km or less. Depth is important because the source of

radon should be on the surface because its half-life is 3.82 days. The results are shown in Figure 18 and Table 11.

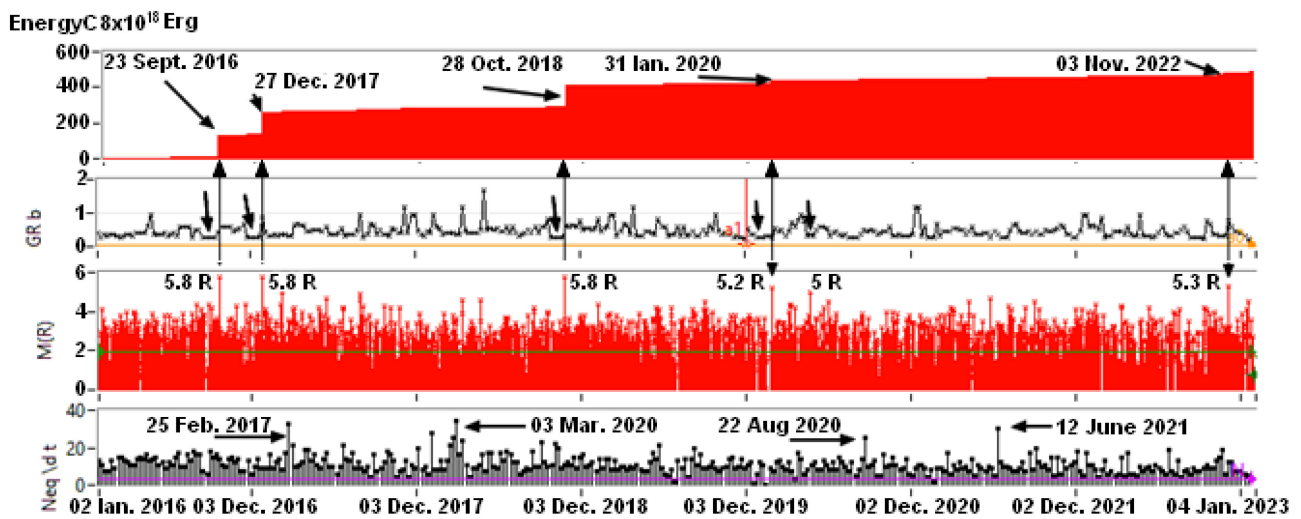


Figure 16. Cumulative seismic energy, the Gutenberg–Richter parameter ‘b’, seismicity, and the number of earthquakes produced in a 7-day interval.

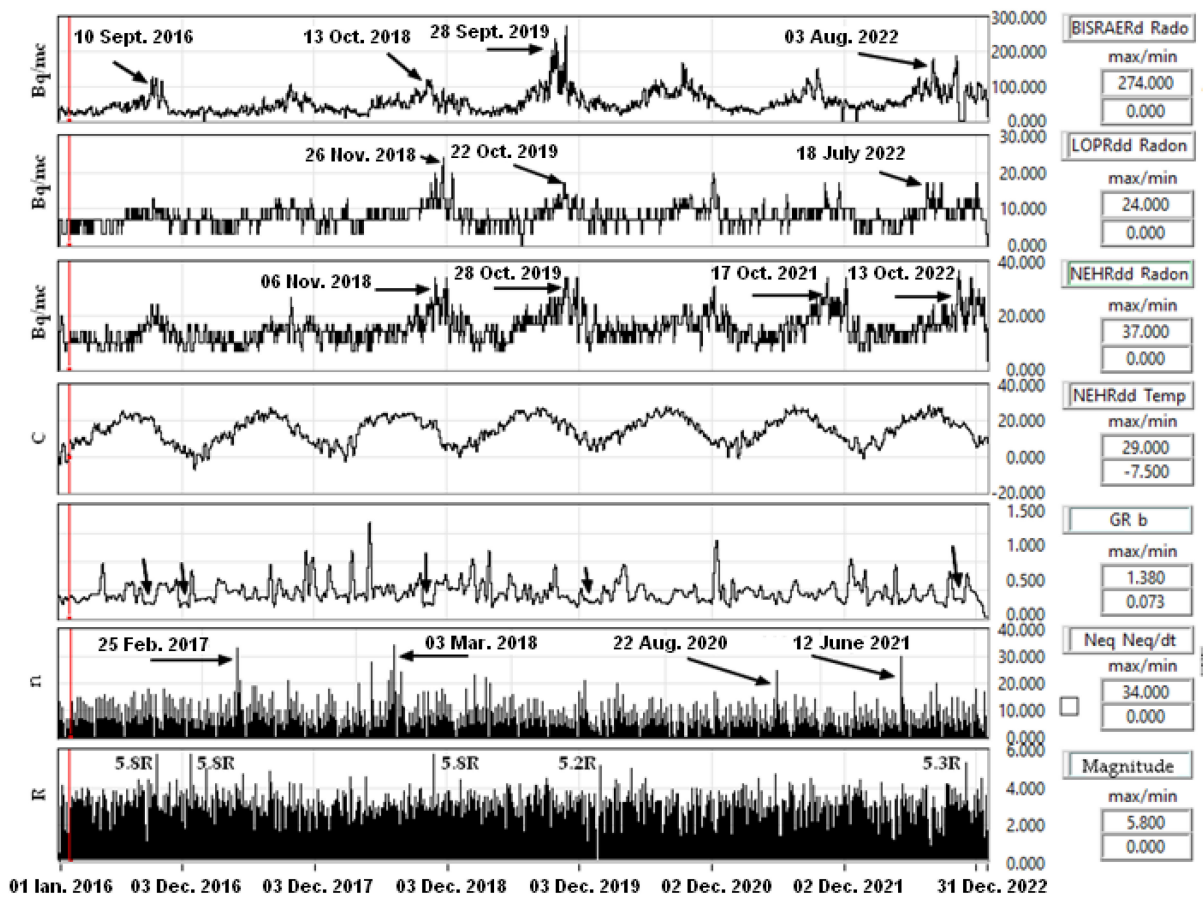


Figure 17. Evolution of radon level, temperature, and seismicity in Vrancea; time windows of 7 days, 2016–2022.

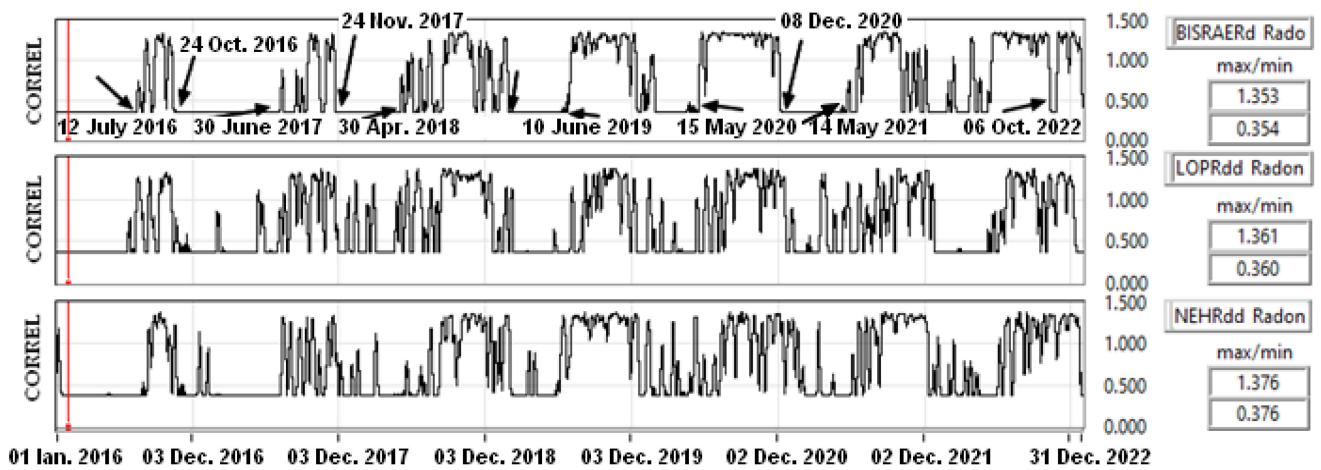


Figure 18. CORREL between GR b (Gutenberg–Richter law) and radon BISRAERs, LOPRdd, and NEHRdd.

Table 11. Correlation factor between ‘b’ parameter and radon in BISRAERd, LOPRdd, and NEHRdd, 2016–2022; time windows of 7 days.

Station, 2016–2022	Mean	Standard Deviation	Mean	Standard Deviation SD
	H > 20 km		H < 20 km	
BISRAERd	0.3541	30.9621	0.3562	30.9617
LOPRdd	0.3707	2.7410	0.3703	2.7410
NEHRdd	0.3766	5.1496	0.3751	5.1495

Correlation of ‘b’ parameters between crustal and deep seismicity for Vrancea using a sliding time window of 7 days is shown in Figure 19, where mean = 0.8767 and SD = 0.4508.

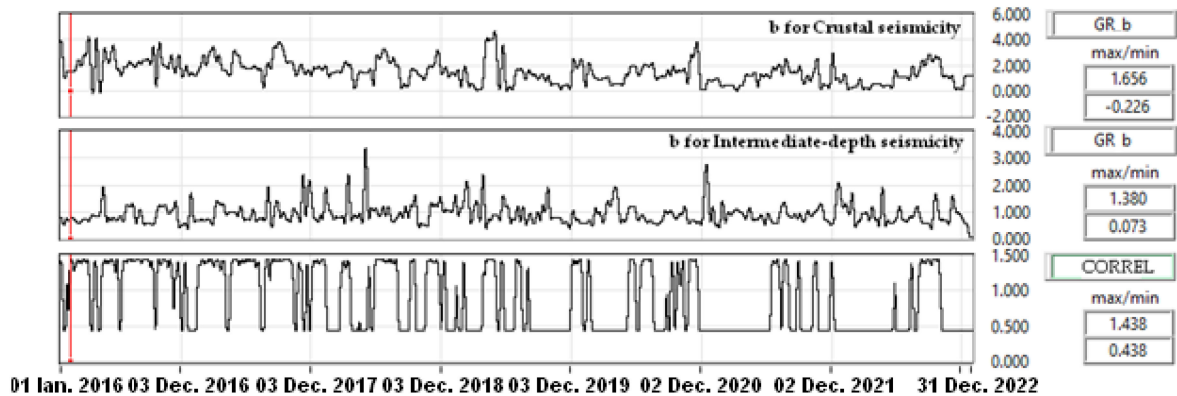


Figure 19. Correlation between b from the Gutenberg–Richter law for Vrancea crustal and deep seismicity.

3.8. Case Study: Radon Variations and Climate Change

Integrating the time series from Figure 17, we obtained the radon variations from Figure 20. We observed a continuous increase in radon level along with the temperature, which we can interpret as an effect of climate change.

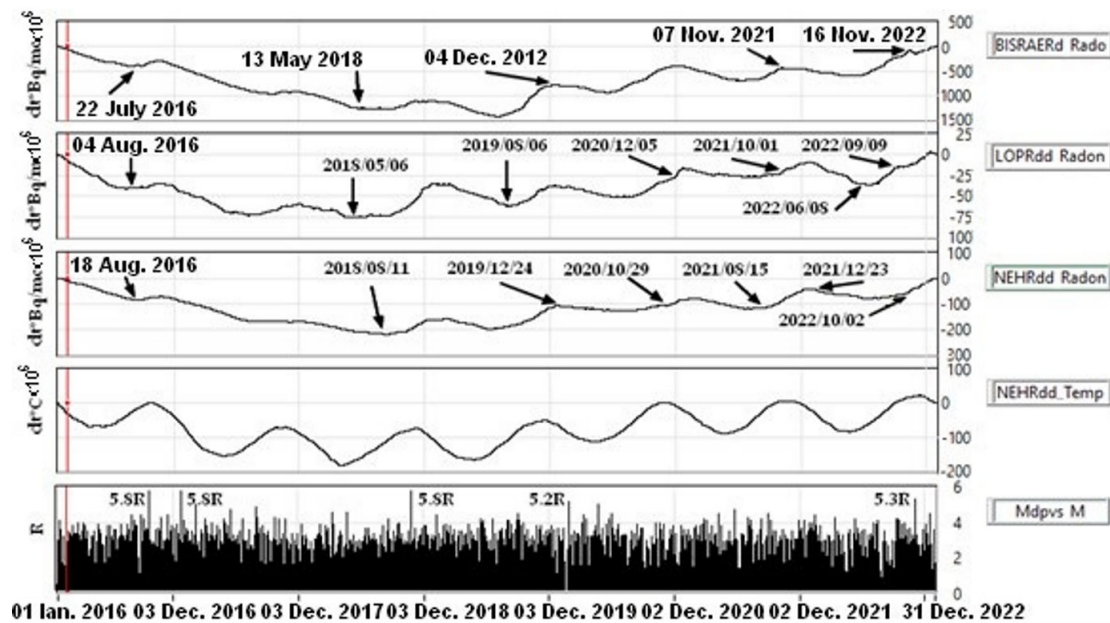


Figure 20. Annual variations of radon integrated and Vrancea seismicity, 2016–2022.

4. Conclusions

From the data presented, it is not possible to establish an exact relationship between the anomalies of radon emissions and seismicity, but evaluations can be made that can be completed with forecasts. Radon level recording depends on environmental factors, location, and installation area. For this reason, the results presented in different articles for different domains may be different. An example has already been mentioned regarding the evolution of radon in LOPRdd, RMGVdd, SAHRdd, and BISRAERd (higher values in summer) and for SURLdd, NEHRdd, and PANCdd (higher values in winter) (Figures 11, 13 and 14). We chose monitoring positions near geological faults, but it is not enough because they may not be active for gas emission. The investigation area was Vrancea (the curvature area of the Carpathian Mountains), which is characterized by deep earthquakes (Table 10). Table 11 shows that the mean value of the correlation factors determined in a 7-day sliding window, and the corresponding SDs were close in value for surface and depth earthquakes (correlation between 'b' parameters in Figure 19). These determinations (Table 11) depend a lot on the calculation method and the way the time series were filtered. We first applied a median filter (LabVIEW library) on the time series from Figure 11 for reducing the daily variations and spikes; next, we used a cross-correlation function (LabVIEW library) and obtained the average values and SD. For this reason, it is important to use the same method for all determinations and the analysis of the results to be comparative.

There will always be a degree of uncertainty because the emission of radon and gases in general depends on many factors. For this reason, a validation with other parameters is necessary. Another direction of development of the multidisciplinary monitoring network and its use is the expansion of measurement points and the introduction of the function of locating sources of disturbances. Climate change affects gas emissions, and their effect needs to be mitigated through data analysis, but they are useful for a new direction of research. In each location, we have weather stations that we will use for corrections and also to analyze the effects of global warming along with CO₂.

In presenting the link between the radon level and seismicity, we used the parameters a–b from the Gutenberg–Richter law (Figure 16). We observed that a decrease over a period longer than 18 days of the parameter 'b' from the Gutenberg–Richter law (GR_b) is followed by earthquakes with a magnitude greater than 5 R (Figures 16 and 17) for the Vrancea area. For this reason, there is no general method, and an implementation of an OEF must take into account the particularities of the monitoring area. In our case, the Vrancea area is unique in Europe due to its geological structure and its deep earthquakes.

One of the most important issues in monitoring geophysical parameters is the location where the equipment is installed. In the case of gas emissions, we tried to position our devices on faults or as close to them as possible. In the areas we selected, we made tomographic resistivity and seismic profiles, as shown in Figures 21 and 22 for the station Bisoca (BISRAERd in Tables 1 and 2) located on the Casin–Bisoca fault.

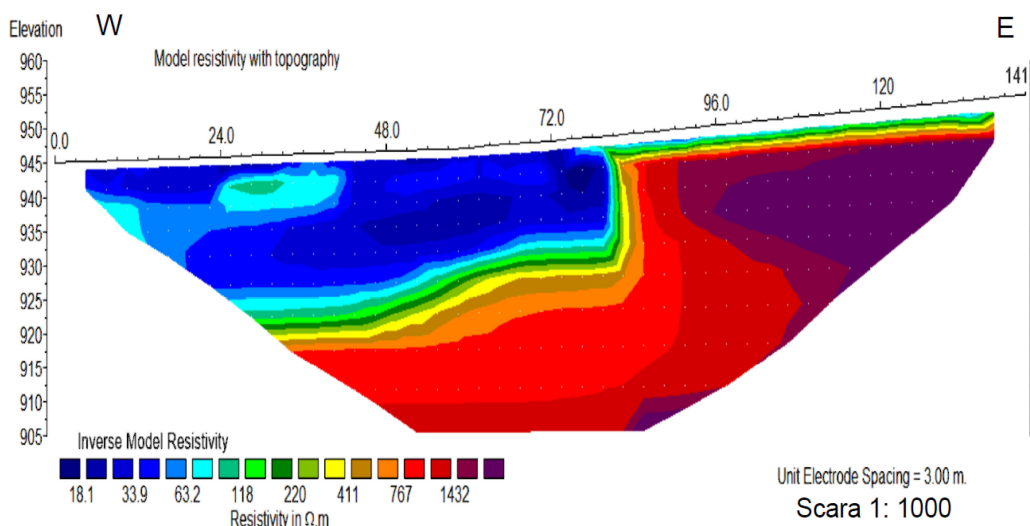


Figure 21. Electrical resistivity tomography section in Bisoca station BISRAERd (project of the Romanian National Authority for Scientific Research, Programe STAR, project 84/2013, made by Getotec Consulting SRL).

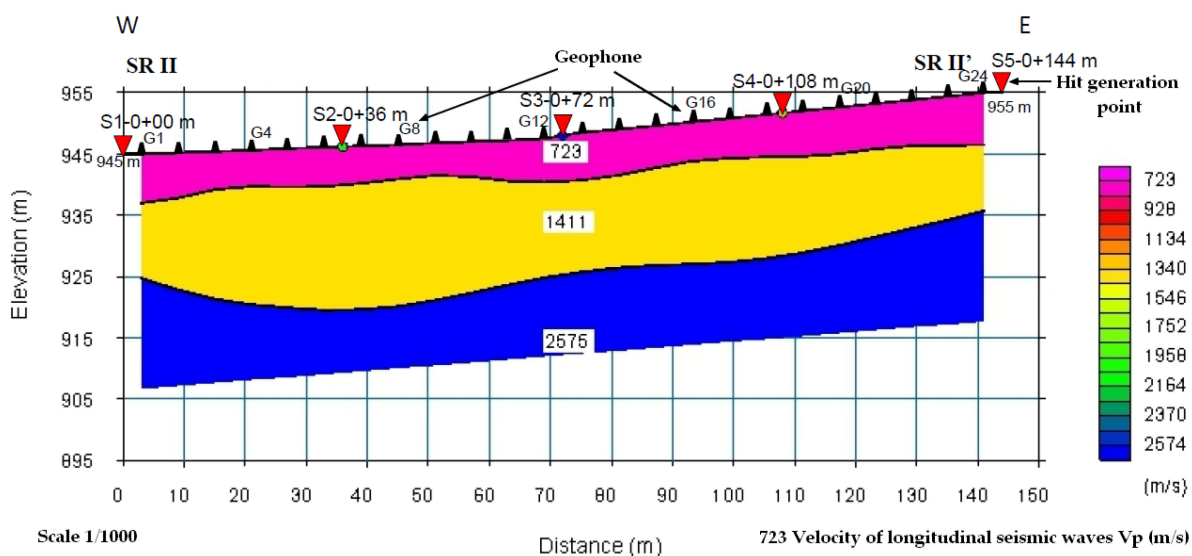


Figure 22. SEISMIC REFRACTION SECTION S.R. II-II in Bisoca station BISRAERd (project of the Romanian National Authority for Scientific Research, Programe STAR, project 84/2013, made by Getotec Consulting SRL).

It is very difficult to determine how radon reaches the surface or where and how it is concentrated. There may be cavities where it concentrates and is released by the increase in outside temperature and the expansion of cracks in the soil or for other reasons. At this site, we made radon measurements in a 2 m deep pit next to a magnetometer. The variations were very small, although there were earthquakes, but their epicenters were in a different area. You should have a large number of instruments installed in the boreholes. This is not possible, because it requires large financial resources, and it is difficult to drill in mountainous areas, where you must also have the necessary infrastructure. For this

reason, the radon detection device was installed in a building connected by a PVC hose to a 2 m deep pit. In this case, it is more difficult to locate the radon source because it can be introduced by air currents. For this reason, we used the wind speed and direction determined by the weather stations installed in all stations. In some cases, this is possible. An example of this can be found in the article [48] that refers to a natural ‘drill’: the volcano Etna. To understand how the radon anomalies were produced, they made a model of radon transport to the surface (source areas and gas carrier velocity). We will address these aspects in a fundamental research project. At this stage, the only data needed for OEF implementation are those that can be predictably correlated, without the need for details on the origin of gas emissions. The only specialized setup for measuring radon and CO₂ is in Figure 3.

One method we plan to use to determine the optimal locations for gas monitoring devices is to deploy a device consisting of at least 16 individual elements, which include a radon and a CO₂ detector, each connected via WiFi, to be distributed in a grid over the target area. The method is similar to that used in resistivity tomography based on electrodes embedded in the ground. We intend to use the resistivity and seismic tomography we have for several sites to correlate with gas emissions. In addition, the monitoring network will soon be expanded to include new instruments (radon, CO₂) that will be installed in 2–3 m deep wells adjacent to the existing seismic sensors.

An improvement in data analysis is achieved by the introduction of artificial intelligence (AI). In general, there are no patterns (at least) for the Vrancea area, but it is worth trying.

Author Contributions: Conceptualization, V.E.T.; methodology, V.E.T. and I.-A.M.; software, V.E.T.; validation, A.M. (Alexandru Marmureanu), N.-S.B., and C.I.; formal analysis, I.-A.M., A.M. (Andrei Mihai), and I.L.; investigation, V.E.T. and I.-A.M.; writing—original draft preparation, V.E.T. and N.-S.B.; correspondent, V.E.T.; supervision, N.-S.B. and I.L. All authors have read and agreed to the published version of the manuscript.

Funding: This paper was funded by MCI grant number PN23360201 (SOL4RISC).

Institutional Review Board Statement: Not applicable.

Informed Consent Statement: Not applicable.

Data Availability Statement: An example of the data is archived at <https://data.mendeley.com/datasets/28kv3gsgcz>, published: 27 September 2022 | Version 2 | <https://doi.org/10.17632/28kv3gsgcz.2> (accessed on 21 May 2023).

Acknowledgments: This paper was carried out within Nucleu Program SOL4RISC, supported by MCI, project no PN23360201; AFROS Project PN-III-P4-ID-PCE-2020-1361, supported by UEFISCDI; and the National Recovery and Resilience Plan, ‘PNRR-III-C9-2022-I5 Establishment and operationalization of Competence Centers’ competition, ‘Competence Center for Climate Change Digital Twin for Earth forecasts and societal redressment (DTEClimate) and The Research Center for Climate Change due to natural Disasters and extreme weather Events-REACTIVE’ projects, contract no. 760008/30.12.2022, code 7/16.11.2022.

Conflicts of Interest: The authors declare no conflict of interest.

References

1. Toader, V.E.; Moldovan, I.A.; Marmureanu, A.; Nastase, E. Monitoring of radon and air ionization in a seismic area. *Rom. Rep. Phys.* **2017**, *69*, 842013.
2. Toader, V.-E.; Nicolae, V.; Moldovan, I.-A.; Ionescu, C.; Marmureanu, A. Monitoring of Gas Emissions in Light of an OEF Application. *Atmosphere* **2020**, *12*, 26. [[CrossRef](#)]
3. Toader, V.-E.; Mihai, A.; Moldovan, I.-A.; Ionescu, C.; Marmureanu, A.; Lingvay, I. Implementation of a Radon Monitoring Network in a Seismic Area. *Atmosphere* **2021**, *12*, 1041. [[CrossRef](#)]
4. Omi, T.; Ogata, Y.; Shiomi, K.; Enescu, B.; Sawazaki, K.; Aihara, K. Implementation of a Real-Time System for Automatic Aftershock Forecasting in Japan. *Seismol. Res. Lett.* **2019**, *90*, 242–250. [[CrossRef](#)]
5. Toader, E.; Moldovan, I.A.; Mihai, A. Forecast Earthquake Using Acoustic Emission. In *International Multidisciplinary Scientific GeoConference Surveying Geology and Mining Ecology Management*; SGEM: Varna, Bulgaria, 2019; Volume 19, pp. 803–811. [[CrossRef](#)]
6. Kachakhidze-Murphy, N.; Kachakhidze, M.; Biagi, P.F. Earthquake Forecasting Possible Methodology. *GESJ Phys.* **2016**, *1*, 102–111.

7. Zechar, J.D.; Marzocchi, W.; Wiemer, S. Operational earthquake forecasting in Europe: Progress, despite challenges. *Bull. Earthq. Eng.* **2016**, *14*, 2459–2469. [CrossRef]
8. Jordan, T.H.; Chen, Y.-T.T.; Gasparini, P.; Madariaga, R.; Main, I.; Marzocchi, W.; Papadopoulos, G.; Yamaoka, K.; Zschau, J. Operational earthquake forecasting: State of knowledge and guidelines for utilization. *Ann. Geophys.* **2011**, *54*, 319–391. [CrossRef]
9. Jordan, T.H.; Marzocchi, W.; Michael, A.J.; Gerstenberger, M.C. Operational earthquake forecasting can enhance earthquake preparedness. *Seismol. Res. Lett.* **2014**, *85*, 955–959. [CrossRef]
10. Tuccimei, P.; Mollo, S.; Soligo, M.; Scarlato, P.; Castelluccio, M. Real-time setup to measure radon emission during rock deformation: Implications for geochemical surveillance. *Geosci. Instrum. Methods Data Syst.* **2015**, *4*, 111–119. [CrossRef]
11. Bauer, S.J.; Gardner, P.; Lee, H. Real Time Degassing of Rock during Deformation. In Proceedings of the 50th US Rock Mechanics/Geomechanics Symposium, Houston, TX, USA, 26–29 June 2016; pp. 1–7.
12. Ambrosino, F.; Thinová, L.; Briestenský, M.; Giudicepietro, F.; Roca, V.; Sabbarese, C. Analysis of geophysical and meteorological parameters influencing ²²²Rn activity concentration in Mladeč caves (Czech Republic) and in soils of Phlegrean Fields caldera (Italy). *Appl. Radiat. Isot.* **2020**, *160*, 109140. [CrossRef]
13. Morales-Simfors, N.; Wyss, R.A.; Bundschuh, J. Recent progress in radon-based monitoring as seismic and volcanic precursor: A critical review. *Crit. Rev. Environ. Sci. Technol.* **2020**, *50*, 979–1012. [CrossRef]
14. Ciogescu, O.; Lingvay, D.; Şchiopu, M.; Lingvay, I.; Toader, V.E.; Ionescu, C.; Marmureanu, A. Complex system for prediction, warning of seismic movements and fire prevention following damage to gas installations caused by major earthquakes. In *BOPI Patent Application 02/2021*; a 2020 00500/10-08-2020; OSIM: Singapore, 2021; Volume 2, p. 35.
15. Nava, F.A.; Márquez-Ramírez, V.H.; Zúñiga, F.R.; Lomnitz, C. Gutenberg–Richter b-value determination and large-magnitudes sampling. *Nat. Hazards* **2017**, *87*, 1–11. [CrossRef]
16. Toader, V.E.; Popescu, I.M.; Moldovan, I.A.; Constantin, I. Vrancea seismicity analysis based on cumulative seismic energy. *UPB Sci. Bull. Ser. A Appl. Math Phys.* **2015**, *77*, 297–308.
17. D’Incecco, S.; Petraki, E.; Priniotakis, G.; Papoutsidakis, M.; Yannakopoulos, P.; Nikolopoulos, D. CO₂ and Radon Emissions as Precursors of Seismic Activity. *Earth Syst. Environ.* **2021**, *5*, 655–666. [CrossRef]
18. Zafir, H.; Barbosa, S.; Levintal, E.; Weisbrod, N.; Ben Horin, Y.; Zalevsky, Z. The Impact of Atmospheric and Tectonic Constraints on Radon-222 and Carbon Dioxide Flow in Geological Porous Media—A Dozen-Year Research Summary. *Front. Earth Sci.* **2020**, *8*, 559298. [CrossRef]
19. Schmid, S.M.; Bernoulli, D.; Fügenschuh, B.; Matenco, L.; Schefer, S.; Schuster, R.; Tischler, M.; Ustaszewski, K. The Alpine-Carpathian-Dinaridic orogenic system: Correlation and evolution of tectonic units. *Swiss J. Geosci.* **2008**, *101*, 139–183. [CrossRef]
20. Matenco, L.; Bertotti, G.; Leever, K.; Cloetingh, S.A.P.L.; Schmid, S.M.; Tărăpoancă, M.; Dinu, C. Large-scale deformation in a locked collisional boundary: Interplay between subsidence and uplift, intraplate stress, and inherited lithospheric structure in the late stage of the SE Carpathians evolution. *Tectonics* **2007**, *26*, TC4011. [CrossRef]
21. Radulian, M.; Popescu, E.; Bala, A.; Utale, A. Catalog of fault plane solutions for the earthquakes occurred on the Romanian territory. *Rom Rep. Phys.* **2002**, *47*, 663–686. Available online: <http://scholar.google.com/scholar?hl=en&btnG=Search&q=intitle:CATALOG+OF+FAULT+PLANE+SOLUTIONS+FOR+THE+EARTHQUAKES+OCCURRED+ON+THE+ROMANIAN+TERRITORY#0> (accessed on 21 May 2023).
22. Radulian, M.; Măndrescu, N.; Panza, G.F.; Popescu, E.; Utale, A. Characterization of Seismogenic Zones of Romania. *Pure Appl. Geophys.* **2000**, *157*, 57–77. [CrossRef]
23. Chen, Z.; Li, Y.; Liu, Z.; Wang, J.; Zhou, X.; Du, J. Radon emission from soil gases in the active fault zones in the Capital of China and its environmental effects. *Sci. Rep.* **2018**, *8*, 16772. [CrossRef]
24. Khan, M.A.; Khattak, N.U.; Hanif, M. Radon emission along faults: A case study from district Karak, Sub-Himalayas, Pakistan. *J. Radioanal. Nucl. Chem.* **2022**, *331*, 1995–2003. [CrossRef]
25. Ioannides, K.; Papachristodoulou, C.; Stamoulis, K.; Karamanis, D.; Pavlides, S.; Chatzipetros, A.; Karakala, E. Soil gas radon: A tool for exploring active fault zones. *Appl. Radiat. Isot.* **2003**, *59*, 205–213. [CrossRef]
26. Xuan, P.T.; Duong, N.A.; Van Chinh, V.; Dang, P.T.; Qua, N.X.; Van Pho, N. Soil Gas Radon Measurement for Identifying Active Faults in Thua Thien Hue (Vietnam). *J. Geosci. Environ. Prot.* **2020**, *8*, 44–64. [CrossRef]
27. Shahrokhi, A.; Burgehele, B.D.; Fábán, F.; Kovács, T. New study on the correlation between carbon dioxide concentration in the environment and radon monitor devices. *J. Environ. Radioact.* **2015**, *150*, 57–61. [CrossRef] [PubMed]
28. Toader, V.E.; Ciogescu, O.; Mihai, A.; Lingvay, D.; Borş, A.; Lingvay, I. Complex system for earthquake prediction and protection of gas installations. *EEA Electroteh Electron Autom.* **2020**, *68*, 100–106. [CrossRef]
29. Haquin, G.; Zafir, H.; Ilzyer, D.; Weisbrod, N. Effect of atmospheric temperature on underground radon: A laboratory experiment. *J. Environ. Radioact.* **2022**, *253–254*, 106992. [CrossRef] [PubMed]
30. Kulali, F.; Akkurt, I.; Özgür, N. The Effect of Meteorological Parameters on Radon Concentration in Soil Gas. *Acta Phys. Pol. A* **2017**, *132*, 999–1001. [CrossRef]
31. Ivanova, K.; Stojanovska, Z.; Djunakova, D.; Djounova, J. Analysis of the spatial distribution of the indoor radon concentration in school’s buildings in Plovdiv province, Bulgaria. *Build Environ.* **2021**, *204*, 108122. [CrossRef]
32. Bem, H.; Janiak, S.; Przybył, B. Survey of indoor radon (Rn-222) entry and concentrations in different types of building in Kalisz, Poland. *J. Radioanal. Nucl. Chem.* **2020**, *326*, 1299–1306. [CrossRef]

33. Al-Hilal, M.; Abdul-Wahed, M.K. Soil gas radon measurements for investigating the actual status of seismic quiescence along the bounding fault of the Ghab pull-apart basin in western Syria. *Geofis. Int.* **2018**, *57*, 177–187. [[CrossRef](#)]
34. Megonigal, J.P.; Brewer, P.E.; Knee, K.L. Radon as a natural tracer of gas transport through trees. *New Phytol.* **2020**, *225*, 1470–1475. [[CrossRef](#)] [[PubMed](#)]
35. Jayaratne, E.R.; Ling, X.; Morawska, L. Role of Vegetation in Enhancing Radon Concentration and Ion Production in the Atmosphere. *Environ. Sci. Technol.* **2011**, *45*, 6350–6355. [[CrossRef](#)] [[PubMed](#)]
36. Vrex, A. Automatic Earthquake Recognition and Timing from Single Traces. *Bull. Seismol. Soc. Am.* **1978**, *68*, 1521–1532.
37. Allen, R. Automatic phase pickers: Their present use and future prospects. *Bull. Seismol. Soc. Am. Geosci.* **1982**, *72*, S225–S242. Available online: <https://pubs.geoscienceworld.org/ssa/bssa/article-abstract/72/6B/S225/102172/Automatic-phase-pickers-Their-present-use-and?redirectedFrom=fulltext> (accessed on 28 April 2020). [[CrossRef](#)]
38. Jones, J.P.; van der Baan, M. Adaptive STA–LTA with Outlier Statistics. *Bull. Seismol. Soc. Am.* **2015**, *105*, 1606–1618. [[CrossRef](#)]
39. Gregori, A.; Zmazek, B.; Deroski, S.; Torkar, D.; Vaupoti, J. Radon as an Earthquake Precursor—Methods for Detecting Anomalies. In *Earthquake Research and Analysis—Statistical Studies, Observations and Planning*; InTech: Milton, Australia, 2012; pp. 179–196. [[CrossRef](#)]
40. Hauser, F.; Raileanu, V.; Fielitz, W.; Bala, A.; Prodehl, C.; Polonic, G.; Schulze, A. VRANCEA99-The crustal structure beneath the Southeastern Carpathians and the Moesian platform from a seismic refraction profile in Romania. *Tectonophysics* **2001**, *340*, 233–256. [[CrossRef](#)]
41. Nevinsky, I.; Tsvetkova, T.; Dogru, M.; Aksoy, E.; Inceoz, M.; Baykara, O.; Kulahci, F.; Melikadze, G.; Akkurt, I.; Kulali, F.; et al. Results of the simultaneous measurements of radon around the Black Sea for seismological applications. *J. Environ. Radioact.* **2018**, *192*, 48–66. [[CrossRef](#)]
42. Ptiček Siročić, A.; Kovač, S.; Stanko, D.; Pejak, I. Dependence of concentration of radon on environmental parameters. *Environ. Eng.* **2021**, *8*, 17–25. [[CrossRef](#)]
43. Xie, D.; Liao, M.; Kearfott, K.J. Influence of environmental factors on indoor radon concentration levels in the basement and ground floor of a building—A case study. *Radiat Meas.* **2015**, *82*, 52–58. [[CrossRef](#)]
44. Taşköprü, C.; İçchedef, M.; Saç, M.M. Diurnal, monthly, and seasonal variations of indoor radon concentrations concerning meteorological parameters. *Environ. Monit. Assess.* **2023**, *195*, 25. [[CrossRef](#)]
45. Aquilina, N.; Fenech, S. The Influence of Meteorological Parameters on Indoor and Outdoor Radon Concentrations: A Preliminary Case Study. *J. Environ. Pollut. Control.* **2019**, *2*, 107.
46. Sundal, A.V.; Valen, V.; Soldal, O.; Strand, T. The influence of meteorological parameters on soil radon levels in permeable glacial sediments. *Sci. Total Environ.* **2008**, *389*, 418–428. [[CrossRef](#)] [[PubMed](#)]
47. Dobrovolsky, I.P.; Zubkov, S.I.; Miachkin, V.I. Estimation of the size of earthquake preparation zones. *Pure Appl. Geophys. PAGEOPH* **1979**, *117*, 1025–1044. [[CrossRef](#)]
48. Neri, M.; Ferrera, E.; Giammanco, S.; Currenti, G.; Cirrincione, R.; Patanè, G.; Zanon, V. Soil radon measurements as a potential tracer of tectonic and volcanic activity. *Sci. Rep.* **2016**, *6*, 24581. [[CrossRef](#)]

Disclaimer/Publisher’s Note: The statements, opinions and data contained in all publications are solely those of the individual author(s) and contributor(s) and not of MDPI and/or the editor(s). MDPI and/or the editor(s) disclaim responsibility for any injury to people or property resulting from any ideas, methods, instructions or products referred to in the content.